International Journal of Minerals, Metallurgy and Materials
Volume 29, Number 12, December 2022, Page 2087
https://doi.org/10.1007/s12613-021-2408-x

Invited Review

Review on coal-based reduction and magnetic separation for refractory iron-bearing resources

Qiang Zhang[1,3], *Yongsheng Sun*[1,2,3)✉], *Yuexin Han*[1,2,3)], *Yanjun Li*[1,3)], *and Peng Gao*[1,2,3)]

1) School of Resources and Civil Engineering, Northeastern University, Shenyang 110819, China
2) State Key Laboratory of Rolling and Automation, Northeastern University, Shenyang 110819, China
3) National-local Joint Engineering Research Center of High-efficient exploitation technology for Refractory Iron Ore Resources, Shenyang 110819, China
(Received: 22 September 2021; revised: 28 December 2021; accepted: 28 December 2021)

Abstract: The application of coal-based reduction in the efficient recovery of iron from refractory iron-bearing resources is comprehensively reviewed. Currently, the development and beneficiation of refractory iron-bearing resources have attracted increasing attention. However, the effect of iron recovery by traditional beneficiation methods is unacceptable. Coal-based reduction followed by magnetic separation is proposed, which adopts coal as the reductant to reduce iron oxides to metallic iron below the melting temperature. The metallic iron particles aggregate and grow, and the particle size continuously increases to be suitable for magnetic separation. The optimization and application of coal-based reduction have been abundantly researched. A detailed literature study on coal-based reduction is performed from the perspectives of thermodynamics, reduction kinetics, growth of metallic iron particles, additives, and application. The coal-based reduction industrial equipment can be developed based on the existing pyrometallurgical equipments, rotary hearth furnace and rotary kiln, which are introduced briefly. However, coal-based reduction currently mainly adopts coal as a reductant and fuel, which may result in high levels of carbon dioxide emissions, energy consumption, and pollution. Technological innovation aiming at decreasing carbon dioxide emissions is a new trend of green and sustainable development of the steel industry. Therefore, the substitution of coal with clean energy (hydrogen, biomass, etc.) for iron oxide reduction shows promise in the future.

Keywords: refractory iron-bearing resources; coal-based reduction; iron recovery; equipment; carbon dioxide emissions

1. Introduction

Iron ore is one of the most important strategic resources in modern industry and the lifeblood of the steel industry [1–2]. Iron ore resources are abundant and mainly distributed in Brazil, Australia, Russia, and China, among which Brazil and Australia show a high total iron (TFe) grade for the iron resources [3]. Raw materials with high TFe grade are necessary for ironmaking when adopting the traditional blast-furnace technology [4–5]. However, iron ore resources are being rapidly consumed, and high-TFe-grade iron ores are gradually decreasing [2,6]. For this reason, consideration has been given to the development and utilization of low-TFe-grade, complex refractory iron-bearing resources, such as oolitic hematite, copper slag, nickel slag, and red mud [7–9]. However, conventional beneficiation methods, such as magnetic separation, gravity concentration, and froth flotation, lose their advantages when processing these iron-bearing resources, and achieving good indexes is difficult [7]. These iron-bearing resources are inherently refractory ores, with "inherently refractory" referring to the ores that can only be beneficiated through complex beneficiation technology due to their complex mineralogical composition and texture [10–12]. Therefore, an increasing emphasis has been placed on pyrometallurgy. Magnetization roasting can effectively treat a part of refractory iron-bearing resources [13]; however, numerous iron-bearing resources are not completely suitable for the magnetization roasting process [14–16]. To develop and utilize this part of iron-bearing resources, a process of coal-based reduction and magnetic separation was innovatively proposed [17–23].

In comparison with the blast-furnace ironmaking, gas-based shaft-furnace direct reduction, and smelting reduction processes, which usually require the use of high-TFe-grade sinters, pellets, and lump ores, coal-based reduction has lower requirements for raw materials; low-TFe-grade iron ores, even fine ores, can be adopted [20–22]. In addition, given the complex mineral composition of raw minerals, the coal-based reduction process includes not only the reduction of iron oxides but also that of other minerals and complex reactions between different minerals. Different from the products of direct reduction (direct-reduction iron) and blast-furnace ironmaking and smelting reduction (liquid iron), the product of coal-based reduction is metallic iron powder, which usually has a TFe grade of more than 90wt%, which may replace the scraps in electric arc furnace steelmaking

✉ Corresponding author: Yongsheng Sun E-mail: yongshengsun@mail.neu.edu.cn

[17,24]. The TFe recovery can reach more than 80wt%. Another attractive feature of coal-based reduction is that the untreated non-coking coal can be used instead of coke as a reductant, from lignite with a fixed carbon content of 30wt% to anthracite with a fixed carbon content of 90wt%. Coal-based reduction is a process applying low-end raw materials to produce high-quality iron powder, and it is complementary to the blast-furnace ironmaking and direct-reduction processes.

Coal-based reduction mainly includes two processes: the reduction of iron oxides and the growth of metallic iron particles [22–23,25–27]. In the coal-based reduction process, iron oxides are selectively reduced to metallic iron below the melting temperature of the ores. By controlling the reduction conditions, the metallic iron particles continually aggregate and grow into larger particles suitable for magnetic separation [22,26] (Fig. 1). The reduction product is often cooled by water. Owing to the difference in thermal conductivity, rapid cooling will cause cracking between metallic iron particles and gangue minerals, which is beneficial to the subsequent grinding. Through the coal-based reduction and magnetic separation process, numerous studies have been implemented to recover iron and explore the relevant factors affecting the process indexes, including reduction temperature, reduction time, reductant ratio, magnetic field intensity, etc. Under optimal conditions, after the grinding and magnetic separation of the reduction product, the high-TFe-grade iron powder with a uniform particle size can be obtained [28–30].

In recent years, to promote the development of coal-based reduction technology, numerous researchers have invested considerable effort from different perspectives and achieved great progress. The possible chemical reactions in the process of coal-based reduction were discussed by thermodynamic studies, and the controlling mechanism of reduction rate was further examined through kinetic studies. The formation and growth of metallic iron particles in the reduction process have been intensively investigated. Researchers also attempted to adopt additives to regulate the coal-based reduction process and explore its mechanism. Coal-based reduction industrial equipment has also been developed to a certain extent. Although previous researchers have performed considerable work on coal-based reduction, systematic and intensive reviews are still lacking. This article reviews the literature on coal-based reduction from the above perspectives. Based on the target specified in the Paris Agreement, the green and sustainable development prospects of carbon neutrality are critically discussed. Arranged in a logical order from process principle to industrial application and then to future development, this review will promote the technology development and utilization of refractory iron-bearing resources.

2. Thermodynamic basis of coal-based reduction

The determination of reaction direction and degree is the premise of applying reactions to practical production, which can be solved by thermodynamic analysis [31]. This analysis helps in further understanding the coal-based reduction process and optimizing its conditions.

In the coal-based reduction process, in general, fixed carbon is the main component of coal [17,30]. Therefore, fixed carbon can be regarded as the reductant involved in iron ox-

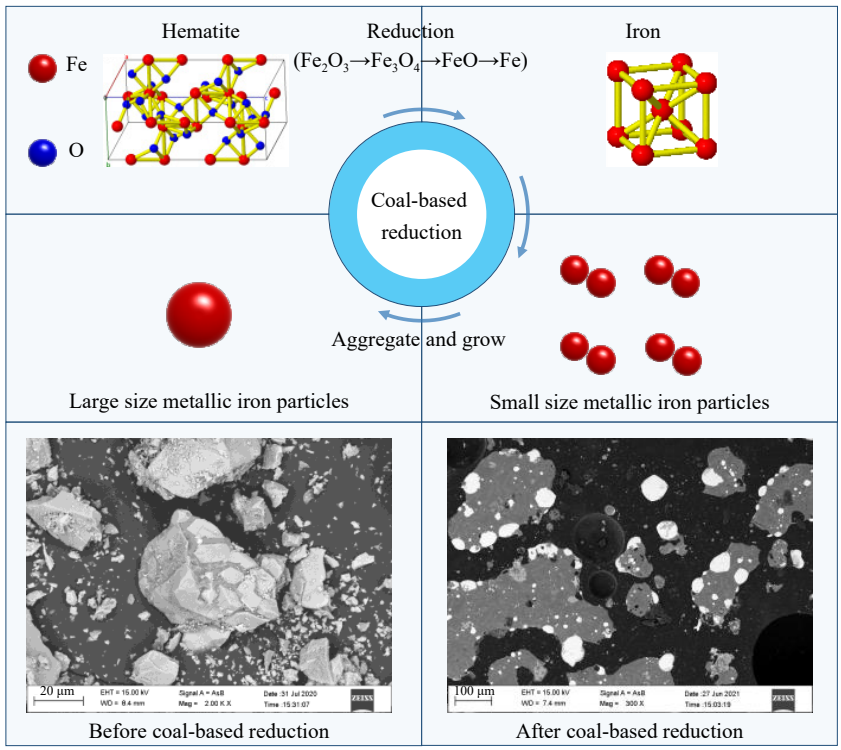

Fig. 1. Schematic of iron oxide reduction, metallic iron particle growth, and microstructure evolution in the coal-based reduction process.

ide reduction. In an air atmosphere, carbon will react as shown in Eqs. (1)–(3) in Table 1 [17]. The Gibbs free energy ($\Delta G^{\ominus}$) was calculated by the Reaction Equations module in HSC chemistry 6.0 software, and the relationship between $\Delta G^{\ominus}$ and T (temperature) was linearly fitted by OriginPro 2022 (Learning Edition) software. The temperature of coal-based reduction is usually above 1273.15 K. Combined with Fig. 2(a), according to the Gibbs free energy criterion of the reaction equilibrium, the conversion of carbon to CO is spontaneous in the standard state [32–33]. With the increase in temperature, the $\Delta G^{\ominus}$ decreases gradually, which is conducive to the conversion of carbon to CO. Notably, CO, as a gas reductant, participates in the reduction of iron oxides [34].

Hematite (Fe_2O_3) cannot be directly reduced to metallic iron (Fe) [33]. Theory and practice have proven that the iron oxide reduction proceeds from a high valence state (Fe^{3+}) to a low valence state (Fe^0) [35–36]. In the coal-based reduction process, the possible reactions of iron oxides are shown in Eqs. (4)–(9) in Table 1, and the relationship between $\Delta G^{\ominus}$ and the temperature of these reactions is presented in Fig. 2(b). Depending on the reduction temperature, the reduction of iron oxides can be divided into two paths [33,36–37]. Below 843.15 K, iron oxide reduction occurs from Fe_2O_3 to magnetite (Fe_3O_4) and then to Fe. No wüstite (FeO) is present in the reduction process because of its instability below 843.15 K. Meanwhile, wüstite is necessarily considered above 843.15 K, and the reduction occurs from Fe_2O_3 to wüstite through Fe_3O_4 and then to Fe.

The Baur–Glaessner diagram in Fig. 3 depicts the reduction thermodynamics of iron oxides. Depending on the temperature and CO concentration (volume ratio of CO to $CO+CO_2$), the phases of iron oxides can be divided into different areas. The stable region of Fe decreases with the increase in temperature, indicating that the utilization rate of CO can be improved at low temperatures. However, given the kinetic and economic factors, the reduction of iron oxides must be carried out at a certain temperature to accelerate the reduction process. The Boudouard reaction of carbon ($C(s) + CO_2(g) = 2CO(g)$) was used to divide the Baur–Glaessner diagram into two areas. With the excess carbon in the coal-based reduction process, the CO concentration is above the equilibrium line, which is conducive to the reduction reaction. Moreover, given that the reduction with CO is exothermic, energy needs not be added to the system to sustain a constant temperature [33]. Fig. 3 denotes that Fe_2O_3 is easy to reduce to Fe_3O_4 despite the extremely low CO concentration. Only when the temperature is higher than 843.15 K, FeO will appear during the reduction of iron oxides [33,38]. As mentioned before, the coal-based reduction temperature is higher than 1273.15 K. Therefore, when the reaction is in equilibrium, iron oxides are reduced to metallic iron.

Thermodynamics analysis showed that during the coal-

Table 1. Main reactions in the coal-based reduction process; data calculated with HSC Chemistry 6.0 software and OriginPro 2022 (Learning Edition) software

Reaction processes	Reaction equations	Number
Carbon gasification	$C(s) + O_2(g) = CO_2(g)$, $\Delta G^{\ominus} = -394.73 - 1.04 \times 10^{-3}T$	(1)
	$2C(s) + O_2(g) = 2CO(g)$, $\Delta G^{\ominus} = -224.97 - 175.16 \times 10^{-3}T$	(2)
	$C(s) + CO_2(g) = 2CO(g)$, $\Delta G^{\ominus} = 169.76 - 174.12 \times 10^{-3}T$	(3)
Iron oxide reduction	$3Fe_2O_3(s) + C(s) = 2Fe_3O_4(s) + CO(g)$, $\Delta G^{\ominus} = 134.01 - 235.30 \times 10^{-3}T$	(4)
	$Fe_3O_4(s) + C(s) = 3FeO(s) + CO(g)$, $\Delta G^{\ominus} = 183.09 - 189.98 \times 10^{-3}T$	(5)
	$FeO(s) + C(s) = Fe(s) + CO(g)$, $\Delta G^{\ominus} = 152.14 - 152.39 \times 10^{-3}T$	(6)
	$3Fe_2O_3(s) + CO(g) = 2Fe_3O_4(s) + CO_2(g)$, $\Delta G^{\ominus} = -35.75 - 61.18 \times 10^{-3}T$	(7)
	$Fe_3O_4(s) + CO(g) = 3FeO(s) + CO_2(g)$, $\Delta G^{\ominus} = 13.34 - 15.86 \times 10^{-3}T$	(8)
	$FeO(s) + CO(g) = Fe(s) + CO_2(g)$, $\Delta G^{\ominus} = -17.62 + 20.83 \times 10^{-3}T$	(9)

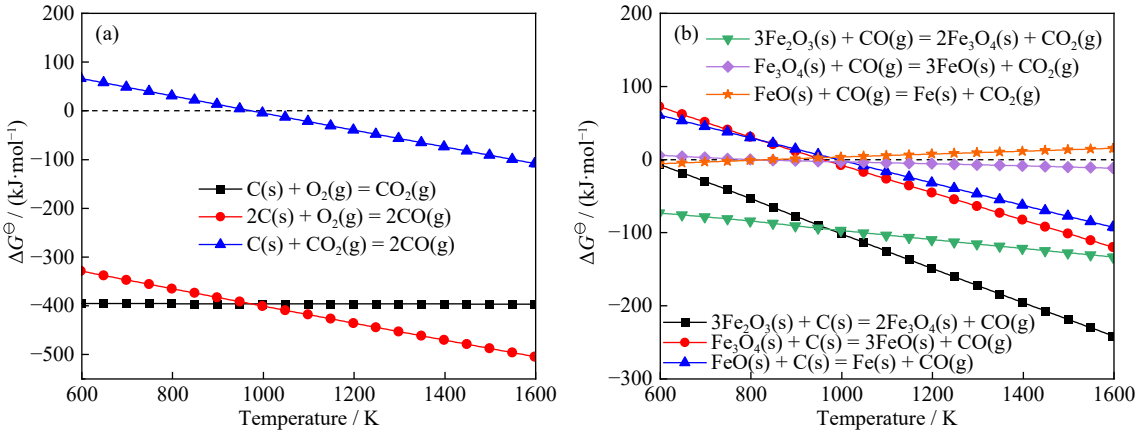

Fig. 2. Relationship between $\Delta G^{\ominus}$ of Eqs. (1)–(9) with temperature: (a) carbon gasification; (b) iron oxide reduction. Data were calculated with HSC Chemistry 6 software.

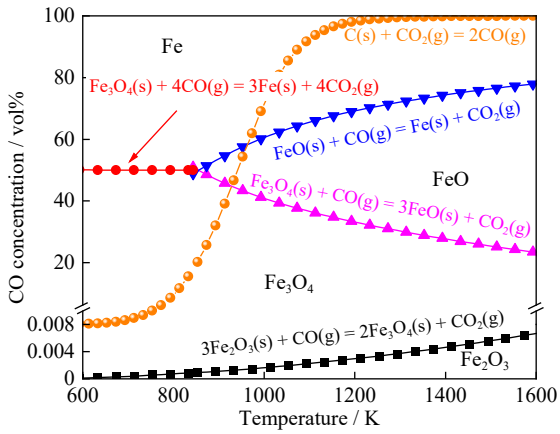

Fig. 3. Baur–Glaessner diagram for the Fe–O–C system, including the Boudouard equilibrium for 100 kPa and a carbon activity of 1 [33].

based reduction process, coal and CO participate in iron oxide reduction in the route of Fe_2O_3→Fe_3O_4→FeO→Fe. CO plays a leading role in the reduction. Thermodynamics is significant and effective. However, although the thermodynamic boundary conditions manifest that the reaction can proceed, it may still be constrained in kinetics. Section 3 discusses reduction kinetic analysis.

3. Reduction kinetics of coal-based reduction

Reaction kinetic analysis is the pillar of the application of chemical reactions in practical industrial production [39–40]; it can determine the influence of reduction conditions on the reduction rate and provide a basis for the optimization of coal-based reduction. Existing studies proved that in the coal-based reduction process, Fe_2O_3 is gradually reduced to Fe, with the intermediate products of Fe_3O_4 and FeO. In addition, considerable kinetic studies have been performed on such reduction processes [21,41–47]. This paper introduces typical kinetic studies from the perspectives of isothermal and non-isothermal reduction kinetics.

3.1. Isothermal reduction kinetics

In general, the analysis of isothermal reduction kinetics is simpler than that of non-isothermal reduction kinetics. The model-fitting method is usually used to determine the reaction kinetic mechanism when analyzing the reaction kinetics under isothermal conditions [21,41–43]. The isothermal kinetics results of coal-based reduction are described below (Table 2).

Under different C/O molar ratios, the results of Sun *et al.* [41] suggested that the effect of temperature on reduction was more significant than that of C/O molar ratios. Given the different main substances involved in the reduction reactions at each stage, the reduction process can be described in three stages with various kinetic mechanisms. Fe_2O_3 was reduced to Fe_3O_4 in the initial stage. Fe_2O_3, Fe_3O_4, and FeO were reduced to Fe in the middle stage. The rate controlling mechanism of these two stages was the interfacial chemical reaction. Fayalite (Fe_2SiO_4) and hercynite ($FeAl_2O_4$) were reduced to Fe in the final stage, with the rate controlling mechanism of solid-state diffusion.

In another study, Sun *et al.* [21] applied chemical analysis instead of thermogravimetric analysis. The reduction rate rose rapidly in the initial stage. The iron oxides were reduced by coal (controlled by interfacial chemical reaction) and its volatiles (controlled by gas diffusion). As the reduction progressed, the CO generated by the Boudouard reaction fully contacted the particle surface. Thus, the surface chemical reaction became the controlling mechanism of the middle stage. The metallic iron gradually covered the particle surface. As a result, the Boudouard reaction weakened, the carbon dissolution increased, and the contact between carbon and iron oxides was complete. Therefore, the controlling mechanism was transformed into the Boudouard reaction and carbon diffusion in the final stage.

Prior research showed that the reduction of iron oxides proceeds in steps. For this reason, Ahmed *et al.* [42] conducted the isothermal kinetics for each iron oxide reduction stage using three reductants. In the process of iron oxide reduction, the reduction rate of Fe_2O_3 to Fe_3O_4 was low and changed nonlinearly. The reduction rate of Fe_3O_4 to FeO was controlled by gasification rate and largely depended on the reductant type. The reduction rate of FeO to Fe increased signi-

Table 2. Isothermal kinetics of coal-based reduction

References	Samples	Reductants	Reduction kinetics mechanisms
Sun *et al.* [41]	Oolitic iron ore	Coal	Initial stage: nucleation (Avrami–Erofeev, A_4) model, $g(\alpha) = [-\ln(1-\alpha)]^{1/4}$; Middle stage: chemical reaction model (n = 2), $g(\alpha) = (1-\alpha)^{-1}-1$ for C/O molar ratio of 1.5 and 2.0, chemical reaction model (n = 3/2), $g(\alpha) = (1-\alpha)^{-1/2}$ for C/O molar ratio of 2.5 and 3.0; Final stage: 3-D diffusion model (Zhuralev–Lesokin–Tempelman), $g(\alpha) = [(1-\alpha)^{-1/3}-1]^2$
Sun *et al.* [21]	Oolitic iron ore	Coal	Initial stage: gas diffusion and interfacial chemical reaction mechanisms; Middle stage: surface chemical reaction; Final stage: solid state diffusion and boundary reaction
Ahmed *et al.* [42]	Hematite iron ore	Graphite, charcoal, and coke	Fe_2O_3 to Fe_3O_4: Not applicable (N. A); Fe_3O_4 to FeO: reduction rate controlled by gasification reaction; Fe_3O_4 to FeO: N. A
Yuan *et al.* [43]	Hematite iron ore	Coke, charcoal, and biomass	Gasification diffusion (Jander equation), $g(\alpha) = [1-(1-\alpha)^{1/3}]^2$

Notes: α is the reduction degree; $g(\alpha)$ is the integral form of the kinetics mechanism function; n is the type of reaction kinetics mechanism.

ficantly, which may be due to the catalytic effect of freshly formed Fe on the carbon gasification reaction.

Yuan *et al.* [43] attempted to reduce iron ore with biomass to alleviate environmental pollution. They compared the isothermal reduction kinetics of iron ore with coke, charcoal, and biomass as the reductant. The results showed that at 1173.15 K, Fe_2O_3 can be reduced to Fe faster with biomass. Meanwhile, at 1473.15 K, the close reduction rate values were observed for the three reductants. Yuan *et al.* [43] considered that the reduction of iron ore by these reductants was mainly controlled by gasification diffusion. The reduction rate can be characterized by the interface reaction kinetic model. The biomass was verified as a promising reductant for iron ore.

3.2. Non-isothermal reduction kinetics

A part of iron oxides is reduced before reaching the preset temperature when conducting isothermal reduction kinetics [42]. Thus, the non-isothermal reduction kinetic analysis must be performed to avoid this situation. The non-isothermal reduction kinetics of iron oxides is briefly introduced below, and the results are summarized in Table 3.

Table 3. Non-isothermal kinetics of coal-based reduction

References	Samples	Reductants	Reduction kinetics mechanisms
Hammam *et al.* [44]	Hematite iron ore	Coal and charcoal	Initial stage: gas diffusion, $g(\alpha) = \alpha^2$; Final stage: nucleation (Avrami–Erofeev, A_2) model, $g(\alpha) = [-\ln(1-\alpha)]^{1/2}$
Sun *et al.* [45]	Oolitic iron ore	Coal	3-D diffusion model (Zhuralev–Lesokin–Tempelman), $g(\alpha) = [1-(1-\alpha)^{1/3}]^2$
Sah and Dutta [46]	Hematite iron ore pellets	Coal	Initial stage: gas diffusion; Final stage: mixed mechanism of gas diffusion and chemical reaction processes
Huang *et al.* [47]	Iron oxidized pellets	Coal	3-D diffusion model (Ginstling–Brounshtein), $g(\alpha) = 1 - 2\alpha/3 - (1-\alpha)^{2/3}$

Hammam *et al.* [44] showed that when the coal was used as the reductant, the reduction route of iron ore was $Fe_2O_3 \rightarrow Fe_3O_4 \rightarrow FeO \rightarrow Fe$. However, when charcoal was used as the reductant, no Fe_3O_4 was present in the reduction process. The non-isothermal reduction kinetic analysis indicated that the controlling mechanisms of the two reductants were the same, i.e., the gas diffusion model in the initial stage and the nucleation model in the final stage.

Sun *et al.* [45] pointed out that the gangue minerals in oolitic iron ore would react with FeO during the coal-based reduction. They recognized that the reduction order of iron oxides was $Fe_2O_3 \rightarrow Fe_3O_4 \rightarrow FeO$ ($FeAl_2O_4$, Fe_2SiO_4)$\rightarrow$Fe [41,45]. The kinetic mechanism function of non-isothermal reduction was the 3-D diffusion model (Zhuralev–Lesokin–Tempelman). Compared with the reduction of FeO to Fe, the activation energy of $FeAl_2O_4$ and Fe_2SiO_4 to Fe was higher, which implied that this reduction was more difficult to achieve.

Sah and Dutta [46] pelletized the high-TFe-grade hematite iron ore (TFe: 66.90wt%) with two kinds of coal and explored the non-isothermal reduction kinetics by thermogravimetric analysis. They observed that in the initial reduction stage, the activation energy was low (0.86–8.82 kJ/mol), and the reduction was controlled by gas diffusion, which is also a widely confirmed phenomenon [48–49]. In the later reduction stage, the activation energy increased (12.37–38.32 kJ/mol), and the controlling mechanism changed to a mixed mechanism of gas diffusion and chemical reaction processes.

Conventional heating has low energy transfer efficiency and poor kinetic conditions, whereas the competitive advantage of microwaves was evident. Huang *et al.* [47] discussed the application of microwave in the reduction of iron-oxidized pellets. The reduction process can be divided into two stages (Stage I: 827–1073 K, Stage II: 1093–1323 K), and the reaction mechanism obeyed the diffusion-controlled model. Analysis of the reduction mechanism revealed that the CO generated by the Boudouard reaction of coal dominated the reduction process. Microwaves can reduce the activation energy and improve the reduction process.

From the kinetic analysis results, given that iron oxides are gradually reduced to metallic iron, the kinetic mechanisms at different stages vary. In the initial stage of reduction, CO is generated by the Boudouard reaction of coal and iron crystal nuclei are formed first. And this process is mainly controlled by a gas diffusion mechanism and a random nucleation mechanism. As the reduction progresses, metallic iron particles continually grow, and the kinetic mechanism related to gas and solid diffusion becomes the main controlling mechanism.

4. Formation and growth of metallic iron particles

An appropriate particle size range is an important condition for the effective magnetic separation of metallic iron and slag [50–52]. The reduction of iron oxides to metallic iron is a prerequisite for the growth of metallic iron particles. Therefore, the evaluation of coal-based reduction should not only characterize the formation of metallic iron by metallization degree but also characterize the growth of metallic iron particles [20,52–54], which has been systematically and comprehensively investigated.

4.1. Formation of metallic iron phase

During the coal-based reduction process, the formation of the metallic iron phase is affected by factors, such as reduction temperature, reduction time, type and dosage of reductant, and additives [25,55–59].

In general, the reduction temperature and time have a great influence on the metallization degree. Sun *et al.* [25] dis-

covered that under different reduction temperatures, the variation trend of the metallization degree with time was the same. The metallization process consisted of two stages, namely, the increasing (<30 min) and stabilizing (>30 min) stages. Before 30 min, the metallization degree increased rapidly with time and gradually stabilized after 30 min. In addition, as the reduction temperature increased, the time required for the metallization degree to stabilize was shortened, and the maximum value of the metallization degree increased. Yu *et al.* [55] and Li *et al.* [56] obtained similar experimental conclusions; that is, the metallization process was divided into two stages: rapid growth and stability.

Furthermore, with a low reductant dosage, iron oxides cannot be sufficiently reduced to metallic iron, resulting in a low metallization degree. This condition led to the deterioration of magnetic separation indexes. When the reductant dosage was sufficient to reduce the iron-bearing minerals in the raw materials to metallic iron, the reductant dosage continually increased, but the metallization degree did not [57–58]. The reaction behavior of iron oxides also varies with the type of reductant. Ahmed *et al.* [42] reported that given that carbon gasification dominates the reduction process, the reaction behavior is closely dependent on the type of carbon source. Charcoal shows the highest reactivity due to its high activated carbon content. Kamijo *et al.* [60] observed that the less volatile matter in coal, the higher the metallization degree of raw materials. This finding may be due to the involvement of fixed carbon in coal in reduction, whereas volatile matter cannot effectively participate in the same process. Yu *et al.* [24] explored the effects of different types of coal on the reduction and magnetic separation of high-phosphorus oolitic hematite ore. The results indicated that when coarse and medium coal was used, bitumite and lignite exhibited a better TFe recovery compared with anthracite, and this advantage disappeared with the decrease in coal particle size. In addition, the TFe grade of iron powder increased with the increase in fixed carbon content and decreased with the decrease in coal particle size. The size of metallic iron grains decreased with the decrease in fixed carbon content in coal and coal particle size. The experiment of Priyadarshi *et al.* [61] also supported that a better reduction effect can be obtained when using a reductant with high fixed carbon content. To date, the application of coal with high fixed carbon content for coal-based reduction is beneficial to improving the reduction behavior of iron oxides and enhancing product quality.

The influence of additives on the formation of the metallic iron phase will be explained in detail later.

4.2. Growth of metallic iron particles

The high metallization degree does not mean that the generated metallic iron particles are suitable for magnetic separation. The growth of metallic iron particles in coal-based reduction must also be explored. A convenient and effective process is the evaluation of the particle size of metallic iron particles by optical image analysis [26,53,62–64]. Through software, the scanning electron micrograph is processed into a binary image, and the particle size is measured and counted (Fig. 4).

Gao *et al.* [53] applied digital image processing technology to analyze the particle size of metallic iron particles and based on this step, drew the cumulative particle size curves for different reduction temperatures and times. Sun and coauthors [26,62–63] investigated the size distribution behavior of metallic iron particles during the coal-based reduction of iron ore. The results presented that the particle size can be controlled by adjusting the reduction conditions [62]. In their previous research, Sun *et al.* [63] adopted the exponential decay function and Rosin–Rammler equation to fit the size frequency distribution curves and the cumulative passing percentage of metallic iron particles, respectively. In subsequent research, the size frequency distribution of metallic iron particles was well fitted by the power function, and the cumulative distribution of metallic iron particles was well fitted by the cumulative distribution function of lognormal distribution [26]. Yu *et al.* [55] revealed that the DoseResp sigmoidal function can be used to characterize the particle size distribution of metallic iron particles during the coal-based reduction of ferronickel slag.

Evidence from several experimental studies has established that the size of metallic iron particles has a significant effect on product quality. Extremely fine particle size will cause magnetic agglomeration during the magnetic separation process, resulting in a decline in product quality [65–66].

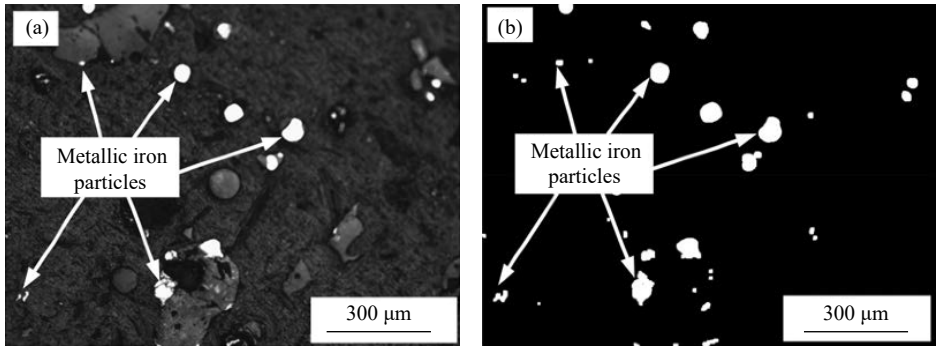

Fig. 4. Optical image analysis for size measurement of metallic iron particles: (a) original metallography and (b) binary metallography [62]. Reprinted by permission from Spring Nature: *Min. Metall. Explor.*, Particle size distribution of metallic iron during coal-based reduction of an oolitic iron ore, Y.X. Han, Y.S. Sun, P. Gao, Y.J. Li, and Y.F. Mu, Copyright 2014.

Only when the metallic iron particles grow to a certain particle size, the metallic iron particles and slag can be well dissociated during the grinding process and the iron can be recovered by magnetic separation. The magnetic separation experiments of Gao *et al.* [53] showed that the separation indexes were closely related to the change in particle size. The larger the metallic iron particles, the easier the separation of metallic iron particles from the slag. However, excessive particle size will increase the cost of reduction and grinding. Therefore, a suitable particle size range is very important, but it has not been determined. The relationship between metallic iron particle size and magnetic separation indexes still lacks exploration and further research.

The growth of metallic iron particles must be controlled to obtain good process indexes. Recently, to deeply understand the formation and growth of metallic iron particles during the reduction process, scientists conducted several studies to explore the growth kinetics of metallic iron particles. Several previous studies are summarized in Table 4 and discussed in more detail below.

Table 4. Growth kinetics of metallic iron particles during the reduction of iron oxides

References	Samples	Stages	Growth kinetics mechanisms	Kinetics parameters
Sun *et al.* [27]	Oolitic iron ore	1423 K ≤ T ≤1523 K, 20 min ≤ t ≤ 50 min	$D^{1/1.3759} = 922.05\exp(-103.18 \times 10^3/RT)t$	n = 1.3759±0.0374, Q = 103.18 kJ/mol, K = 922.05
Sun *et al.* [25]	Oolitic iron ore	Stage I: 1423 K ≤ T ≤ 1300 K, t ≤ 30 min; Stage II: 1423 K ≤ T ≤1573 K, 30 min ≤ t	Stage I: $D^{14.95} = 7.88 \times 10^{37}\exp(-631.41 \times 10^3/RT)t$; Stage II: $D^{4.08} = 4.34 \times 10^9\exp(-184.11 \times 10^3/RT)t$	Stage I: n = 14.95, Q = 631.41 kJ/mol, K = 7.88 × 10^{37}; Stage II: n = 4.08, Q = 184.11 kJ/mol, K = 4.34 × 10^9
Zhang *et al.* [67]	Copper slag	1423 K ≤ T ≤1573 K, 30 min ≤ t ≤ 180 min	$D^{1.424} = 20839.38\exp(-116.17 \times 10^3/RT)t$	n =1.424 ± 0.07855, Q = 116.17 kJ/mol, K = 20, 839.38
Li *et al.* [56]	Nickel slag	Stage I: 1373 K ≤ T ≤ 1523 K, 10 min ≤ t ≤ 30 min; Stage II: 1373 K≤ T ≤ 1523 K, 30 min ≤ t ≤ 60 min	Stage I: $D^{1/0.4697} = 3.81 \times 10^8\exp(-249.04 \times 10^3/RT)t$; Stage II: $D^{1/1.0774} = 217.30\exp(-92.93 \times 10^3/RT)t$	Stage I: n = 0.4697, Q = 249.04 kJ/mol, K=3.81×10^8; Stage II: n = 1.0774, Q = 92.93 kJ/mol, K = 217.30
Yu *et al.* [55]	Ferronickel slag	Stage I: 1473 K ≤ T ≤ 1623 K, t ≤ 40 min; Stage II: 1473 K ≤ T ≤ 1623 K, 40 min < t	Stage I: $D = (30.33 \pm 1.92)t^{0.496\pm0.019}\exp(-(52.482 \pm 4.448) \times 10^3/RT)$; Stage II: $D = (21.30 \pm 1.45)t^{0.168\pm0.043}\exp(-(26.429 \pm 3.295) \times 10^3/RT)$	Stage I: n = 2.016 ± 0.076, Q = 52.482 ± 4.448 kJ/mol, K = 30.33 ± 1.92; Stage II: n = 5.960 ± 2.060, Q = 26.429 ± 3.295 kJ/mol, K = 21.30±1.45

Notes: t is the reduction time, min; D is the particle size, mm; R is the universal gas constant, 8.314 kJ/mol; n is the particle growth index; Q is the apparent activation energy, kJ/mol; K is the pre-exponential factor, min^{-1}.

Sun *et al.* [27] studied the growth characteristics of metallic iron particles during the coal-based reduction of oolitic iron ore. They observed that iron minerals on the surface were first reduced to form metallic iron nuclei, which accumulated with each other and grew and separated from the surface under the action of interfacial tension. In accordance with the principle of minimum Gibbs free energy, most of the metallic iron particles grew into quasi-spheres. Moreover, increasing the reduction temperature and time within a certain range can significantly improve the particle size of metallic iron particles. However, the growth kinetic model established in this research [27] is different from that in another research [25]. Sun *et al.* [25] observed that the growth of metallic iron particles can be characterized via two stages. In the first stage (before 30 min), the growth of metallic iron particles was controlled by the chemical reaction of iron oxide reduction to metallic iron. Meanwhile, in the second stage (after 30 min), the growth of metallic iron particles was controlled by surface diffusion and metallic iron diffusion.

Zhang *et al.* [67] adopted optical image analysis to investigate the growth behavior of metallic iron particles. They explored the growth process of metallic iron particles under isothermal and non-isothermal conditions. The results showed that under isothermal conditions, the growth rate exhibited an S-shaped growth with time. Under non-isothermal conditions, the growth rate increased exponentially with temperature. On the basis of the Hillert kinetics model, Zhang *et al.* [67] established the growth kinetics model of metallic iron particles.

The coal-based reduction of nickel slag conducted by Li *et al.* [56] indicated that the growth of metallic iron particles can be divided into two stages with a boundary of 30 min. In stage I, the metallic iron particles nucleated, and the weak diffusion capability of metallic iron particles limited their growth. As the reduction proceeded, the metallic iron particles grew rapidly in stage I. The kinetic analysis showed that the metallic iron particles more easily grew in stage II given the higher content of metallic iron in this stage. As a result, the driving force of crystal growth was greater.

Yu *et al.* [55] researched the growth kinetics of high-TFe-grade ferronickel slag during coal-based reduction. During the rapid formation period (stage I), metallic iron particles with small particle sizes had large surface energy, forming a strong driving force for particle growth that caused the rapid growth of metallic iron particles. In the aggregation growth period (stage II), the growth rate of metallic iron particles decreased significantly and was limited by the interface chemical reaction. At this stage, small metallic iron particles gradually aggregate into large metallic iron particles.

In summary, at the initial growth stage, the size of metallic iron particles increases rapidly, and as the reduction proceeds, the growth rate gradually slows down. In this process, temperature plays a decisive role in its growth.

5. Action of additives

The coal-based reduction process can be optimized by selecting an appropriate number of additives. To date, the commonly used additives include CaF_2, $NaCO_3$, CaO, $MgCO_3$, etc. [59,68–71]. These additives can improve the process indexes of coal-based reduction and magnetic separation, promote the formation and growth of metallic iron particles, and improve product quality.

5.1. Improvement of the process indexes

Refractory iron ores often contain a number of gangue minerals, especially SiO_2 and Al_2O_3 [59,72]. These gangue minerals easily react with FeO to form intermediate products ($FeAl_2O_4$ and Fe_2SiO_4) [73]. Previous kinetic studies showed that $FeAl_2O_4$ and Fe_2SiO_4 are difficult to reduce to Fe, which is not conducive to coal-based reduction. To improve the process indexes of coal-based reduction and magnetic separation, numerous researchers explored the utilization of additives, such as Na_2CO_3, $MgCO_3$, CaO, and CaF_2, and systematically studied their action mechanism [59,68–70,74]. Table 5 exhibits that the appropriate utilization of additives can significantly increase the TFe grade and recovery.

In the coal-based reduction process, Na_2CO_3 and $MgCO_3$ are first decomposed to form Na_2O and MgO, respectively [59,70]. Table 6 shows the possible reactions of Na_2O, MgO, and CaO with gangue minerals and intermediate products [59,69,73,77]. Fig. 5 presents the $\Delta G^{\ominus}$ of these reactions as a function of temperature. Within the coal-based reduction temperature range, on the one hand, these additives can react with gangue minerals to prevent the reaction between gangue minerals and FeO to increase the metallization degree [70]. On the other hand, additives can react with $FeAl_2O_4$ and Fe_2SiO_4 to substitute FeO, and the newly formed FeO can subsequently be reduced to Fe [74,78]. The action mechanism of CaF_2 is more complicated. The radius of F^- is close to that of O^{2-}; thus, F^- can substitute the O^{2-} in the silicon oxygen tetrahedron to disintegrate the silicon oxygen complexions, as shown in Eq. (22) [59,69]. In addition, when the basicity is high, F^- can sever the ionic bond between Al^{3+}, Ca^{2+}, and silicon oxygen tetrahedron (Eqs. (23)). This phenomenon decreases the surface tension of the samples and system viscosity, optimizes the contact conditions between the samples and pulverized coal, promotes the reduction reactions, and decreases the resistance to aggregation and growth of metallic iron particles [59,69]. Moreover, additives can promote the Boudouard reaction of carbon and improve the generation rate of CO to catalyze the reduction of iron oxides and improve the process indexes [76,79–80].

Table 5. Increase in the process indexes of coal-based reduction and magnetic separation by additives

References	Additives	Increase in metallization degree	Increase in TFe grade	Increase in TFe recovery
Gao *et al.* [59]	CaF_2 (6wt%)	6.19wt%	7.48wt%	3.23wt%
	Na_2CO_3 (5wt%)	4.99wt%	2.51wt%	3.04wt%
	$MgCO_3$ (4wt%)	5.59wt%	1.57wt%	0.69wt%
Zhang *et al.* [73]	CaO (8wt%)	5.10wt%	2.82wt%	4.80wt%
	CaO (8wt%) + Na_2CO_3 (3wt%)	6.60wt%	3.79wt%	6.30wt%
Han *et al.* [68]	Na_2CO_3 (5wt%)	5.99wt%	2.51wt%	4.04wt%
Long *et al.* [69]	CaF_2 (1.3wt%)	N. A	12.04wt%	8.81wt%
Yang *et al.* [75]	CaO (10wt%)	0.79wt%	3.02wt%	4.26wt%
Bai *et al.* [76]	Na_2CO_3 (10wt%)	N. A	10.40wt%	5.10wt%

Table 6. Main reaction equations of additives that may occur in coal-based reduction

Additives	Reaction equations	Number
Na_2CO_3	$Na_2O(s) + SiO_2(s) = Na_2O{\cdot}SiO_2(s)$	(10)
	$Na_2O(s) + 2FeO{\cdot}SiO_2(s) = 2FeO(s) + Na_2O{\cdot}SiO_2(s)$	(11)
	$Na_2O(s) + Al_2O_3(s) = Na_2O{\cdot}Al_2O_3(s)$	(12)
	$Na_2O(s) + FeO{\cdot}Al_2O_3(s) = FeO(s) + Na_2O{\cdot}Al_2O_3(s)$	(13)
$MgCO_3$	$2MgO(s) + SiO_2(s) = 2MgO{\cdot}SiO_2(s)$	(14)
	$2MgO(s) + 2FeO{\cdot}SiO_2(s) = 2FeO(s) + 2MgO{\cdot}SiO_2(s)$	(15)
	$MgO(s) + Al_2O_3(s) = MgO{\cdot}Al_2O_3(s)$	(16)
	$MgO(s) + FeO{\cdot}Al_2O_3(s) = FeO(s) + MgO{\cdot}Al_2O_3(s)$	(17)
CaO	$CaO(s) + SiO_2(s) = CaO{\cdot}SiO_2(s)$	(18)
	$CaO(s) + 2FeO{\cdot}SiO_2(s) = 2FeO(s) + CaO{\cdot}SiO_2(s)$	(19)
	$CaO(s) + Al_2O_3(s) = CaO{\cdot}Al_2O_3(s)$	(20)
	$CaO(s) + FeO{\cdot}Al_2O_3(s) = FeO(s) + CaO{\cdot}Al_2O_3(s)$	(21)
CaF_2	$(□Si–O–Si□) + 2F^- = (□Si–O–F) + (□Si–F)$	(22)
	$(□Si–O–Ca–O–Si□) + CaF_2 = 2(□Si–O–Ca–F)$	(23)

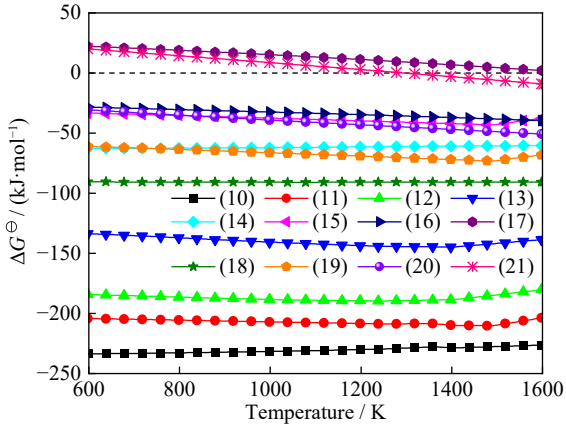

Fig. 5. Relationship between $\Delta G^{\ominus}$ of Eqs. (10) to (21) with temperature; data calculated with HSC Chemistry 6 software.

5.2. Promotion of the growth of metallic iron particles

Large metallic iron particles are conducive to magnetic separation. Therefore, the coal-based reduction process needs to be regulated to promote the growth of metallic iron particles. Researchers consider the utilization of additives to achieve this objective.

During the coal-based reduction process, additives react with gangue minerals to form low-melting compounds, such as $Na_2O{\cdot}SiO_2$, $3CaO{\cdot}2SiO_2{\cdot}CaF_2$, and $CaO{\cdot}SiO_2$ [15,59,69,76,81]. These low-melting compounds form a micro-melting phase under high temperatures in the coal-based reduction process, which can promote the diffusion of crystalline particles and accelerate the formation and growth of iron crystal nuclei [59,68,82]. Li *et al.* [83] reported that the size of metallic iron particles was between 10–20 μm in the absence of sodium salts, and metallic iron particles were closely associated with gangue minerals. After the addition of sodium salts, the average particle size of metallic iron particles increased significantly to 50 μm (Fig. 6). The thermodynamic analysis results of Zinoveev *et al.* [84] showed that during coal-based reduction, the liquid-phase content of red mud increased after the addition of carbonates. Their test results also indicated that the addition of carbonates can significantly increase the size of metallic iron particles. Grudinskii *et al.* [85] observed that in the temperature range of 1273–1473 K, when graphite was used to reduce the iron oxides in red mud, the addition of alkali metal carbonates and alkali metal sulfates can increase the percentage of metallic iron particles with a particle size greater than 0.04 mm, and the facilitation effect of alkali metal sulfates was improved. Bai *et al.* [76,80] noticed that in the reduction process, the addition of Na_2CO_3 can lighten the burden of metallic iron particles surrounded by SiO_2 and promote their growth and aggregation. Xing *et al.* [15] stated that after adding CaF_2 (3wt%), the average diameter of metallic iron particles increased significantly, indicating that CaF_2 is advantageous to the formation, aggregation, and growth of metallic iron particles. However, an appropriate dosage of additives is necessary. An appropriate dosage is required because the excessive micro-melt phase will seriously wrap the iron oxide particles, leading to insufficient reduction and thus decreasing the metallization degree and particle size of the reduction products [59,68,86].

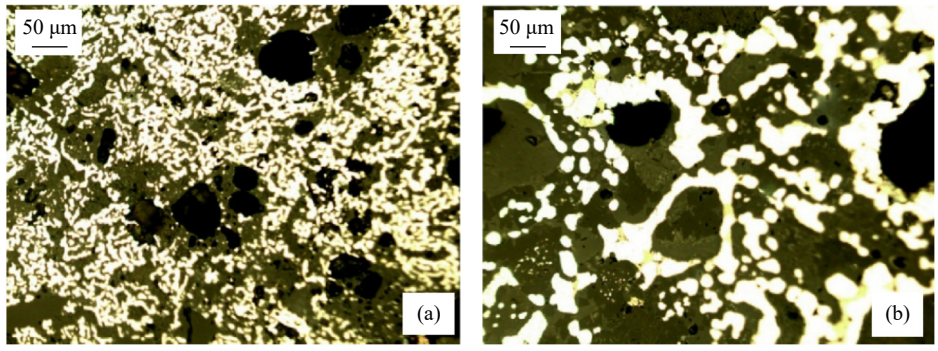

Fig. 6. Promotion of the growth of metallic iron particles by additives: (a) without additives; (b) with 7.5wt% sodium sulfate and 1.5wt% borax [83]. Reprinted from *Int. J. Miner. Process.*, 124, G.H. Li, S.H. Zhang, M.J. Rao, Y.B. Zhang, and T. Jiang, Effects of sodium salts on reduction roasting and Fe–P separation of high-phosphorus oolitic hematite ore, 26-34, Copyright 2013, with permission from Elsevier.

5.3. Enhancement of the product quality

For most types of steel, phosphorus (P) is harmful to the properties of steel and easily result in the cold brittleness of steel [28,72,87]. Moreover, the high P content is not conducive to welding and will increase the susceptibility to welding cracks [88]. Given that P is inevitably contained in refractory iron ores and is easily absorbed by liquid iron, the presence of this element has become a restrictive indicator to enhance the product quality. Therefore, P must be removed from iron powder, which is the coal-based reduction product. Currently, dephosphorization through additives is an effective method for P removal [28,74,89–90]. Three main dephosphorization mechanisms of additives have been recognized [91].

First, the additives will react with SiO_2 and Al_2O_3, as clarified in Eqs. (10) to (21), thereby lessening the promoting effect of SiO_2 and Al_2O_3 on the reduction of fluorapatite [23,28,73,77,86]. Fluorapatite is the main form of P in oolitic hematite ore. Therefore, Sun *et al.* [28] and Zhang *et al.* [73] studied the effect of SiO_2 and Al_2O_3 on the reaction behavior of fluorapatite during coal-based reduction. SiO_2 and Al_2O_3

can promote the reduction of fluorapatite, and the kinetics mechanisms of these reduction processes are $A_{1/3}$ and $A_{1/2}$ nucleation models, respectively. Moreover, the activation energy of fluorapatite reduction catalyzed by SiO_2 was evidently lower than that of Al_2O_3, which suggested that the catalyzation role of SiO_2 was more prominent [28]. Given that the reduction of fluorapatite will produce P_2 gas, liquid iron will absorb a large amount of P_2 gas to form Fe–P alloy, leading to a high P content of the iron powder [73]. Zhang *et al.* [73] proposed that lowering the reduction temperature can delay the melting of metallic iron; at a low reduction temperature, fluorapatite was difficult to reduce [92]. The function of $Ca(OH)_2$ and Na_2CO_3 to inhibit the reduction of fluorapatite in oolitic hematite ore was evaluated by Yu *et al.* [77]. $Ca(OH)_2$ and Na_2CO_3 can consume SiO_2 to constrain the reduction of fluorapatite. $Ca(OH)_2$ can also enhance the melting point and viscosity of the slag, deteriorate the reaction conditions, and suppress the reduction of fluorapatite. Similarly, Zhao *et al.* [86] confirmed the same inhibitory mechanism of $CaCO_3$ on the reduction of fluorapatite. They removed the unreduced fluorapatite through magnetic separation.

The oolitic structure of oolitic hematite ore severely limits its dephosphorization [14]. Therefore, the second dephosphorization mechanism of additives aims to destroy the oolitic structure, which promotes the reduction of iron oxides and the growth of metallic iron particles and increases the liberation degree of minerals in the reduction products [83,93–94]. Then, the iron powder and P-containing minerals can be separated via grinding and magnetic separation. Fig. 7 shows the effect of the dephosphorization agent on the oolitic structure in coal-based reduction. To separate iron and phosphorus from oolitic hematite, Li *et al.* [83] carried out a coal-based reduction with sodium salts and magnetic separation experiments. The results denoted that 7.5wt% sodium sulfate (Na_2SO_4) and 1.5wt% borax ($Na_2B_4O_7$) can markedly ameliorate the magnetic separation effect of Fe and P (dephosphorization rate: 96.1wt%). The sodium salts reacted with gangue minerals to destroy the oolitic structure. This event promoted the reduction of iron oxides and the growth of metallic iron particles, which facilitated the separation of Fe and P. Furthermore, Li *et al.* [93] endeavored to replace a part of NCP additives with lower-price TS additives. These additives reacted with SiO_2 to form silicate minerals and destroyed the oolitic structure. This phenomenon smoothed the contact surface between metallic iron particles and gangue particles, which was helpful for magnetic separation. P was still present in the form of fluorophosphate, and dephosphorization was realized by fine grinding and magnetic separation.

The last dephosphorization mechanism converts P into soluble phosphate, which is easy to remove [80,95–96]. Xu *et al.* [95] confirmed that the P-containing minerals in an oolitic hematite ore from Nigeria were mainly crandallite ($CaAl_3(OH)_6(HPO_4)(PO_4)$) and vauxite ($FeAl_2(PO_4)_2OH\cdot 6H_2O$), with fine particle size and embedded in oolitic hematite ore. They explored the dephosphorization effect of sodium carbonate. Several P-containing minerals (51.64wt%) reacted with Na_2CO_3 and gangue minerals during the reduction process to form water-soluble phosphate, which was dissolved in water during the magnetic separation process. Another part of P-containing minerals (45.16wt%) was not reduced under the action of Na_2CO_3 and entered the tailings during magnetic separation. Yang *et al.* [96] observed that after adding a dephosphorization agent, 38.78wt% of P entered the soluble phosphate, and 56.87wt% entered the aluminosilicate formed by the reaction of the dephosphorization agent, apatite, collophanite, and quartz. Therefore, P and Fe can be separated by magnetic separation. Using Na_2CO_3 (5wt%) as an additive, after coal-based reduction and magnetic separation, the dephosphorization of high-P siderite was significant, and a low-P iron powder was obtained [80]. Bai *et al.* [80] reported that Na_2CO_3 can not only curb the reduction of fluorapatite but also react with insoluble fluorapatite to form soluble phosphate (Eq. (24)).

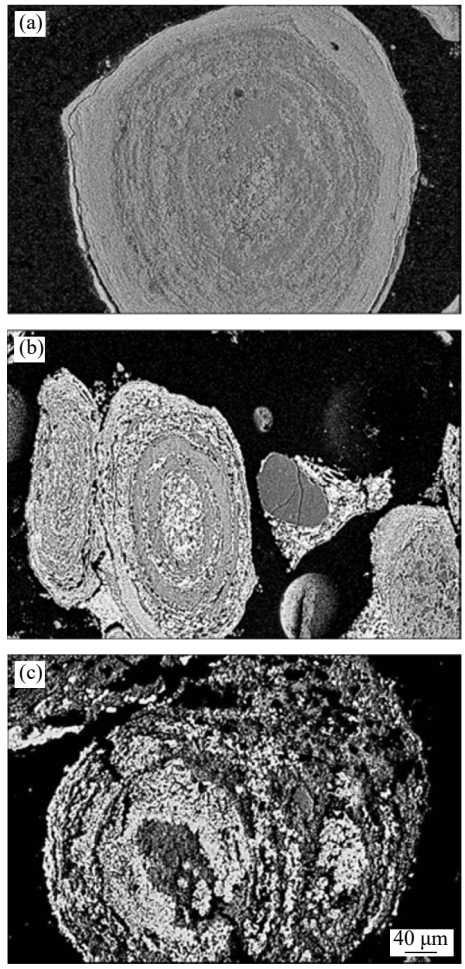

Fig. 7. Microstructure of the raw ore (a), reduction products without a dephosphorization agent (b), and those with a dephosphorization agent (c) [94]. Reprinted from *Trans. Nonferrous Met. Soc. China*, 22, C.Y. Xu, T.C. Sun, J. Kou, Y.L Li, X.L Mo, and L.G Tang, Mechanism of phosphorus removal in beneficiation of high phosphorous oolitic hematite by direct reduction roasting with dephosphorization agent, 2806-2812, Copyright 2012, with permission from Elsevier.

$$Ca_3(PO_4)_2(\text{insoluble}) + 3Na_2CO_3 \rightarrow 2Na_3PO_4(\text{soluble}) + 3CaO + 3CO_2 \quad (24)$$

6. Application and development of coal-based reduction

To date, quantities of studies have been conducted on the application of coal-based reduction and magnetic separation to recover iron from various refractory iron-bearing resources. The results of these studies are summarized in Table 7 and discussed in detail below. The equipment of coal-based reduction is different from that of traditional iron-making and direct-reduction iron. Numerous kinds of equipment are currently used in pyrometallurgy methods. In accordance with the equipment characteristics and requirements of the coal-based reduction process, here, the rotary hearth furnace (RHF) [97–99] and rotary kiln (RK) [100–102] are introduced, which has development potential for coal-based reduction. However, given the requirements of green, low-carbon, and sustainable development, the application of coal-based reduction is seriously limited, and its future application is subject to multitudinous challenges. Its development prospect is discussed and critically prospected.

Table 7. Summary of the coal-based reduction technology applied for refractory iron-bearing resources

References	Samples	Reductants	Reduction conditions			Products	
			Temperature	Time	Dosage of additives and reductants	TFe grade	TFe recovery
Li *et al.* [29]	Copper slag (−74 μm, 90wt%)	Coke (−74 μm, 90wt%)	1573 K	180 min	Coke: 14wt%, CaO: 5.38wt%	96.21%	91.82%
Wang *et al.* [103]	Copper slag (−74 μm, 90wt%)	Lignite (−74 μm, 90wt%)	1523 K	180 min	Lignite: 20wt%, CaO: 8.9wt%	93.64%	88.08%
Wang *et al.* [104]	Copper slag (−100 μm)	Coke (−0.60 mm, 69.20wt%)	1573 K	120 min	Coke: 14wt%, CaO: 6wt%	92.96%	93.49%
Zhou *et al.* [105]	Copper slag (2–4 mm)	Walnut shell (2–4 mm)	1573 K	60 min	Walnut shell char: 15wt%	73.20%	95.56%
Yuan *et al.* [17]	Nickel laterite ore (−2 mm)	Coal (−2 mm)	1548 K	50 min	Slag basicity: 1.0, carbon-containing coefficient: 2.5	34.74%	80.44%
Zinoveev *et al.* [84]	Red mud (−2 mm)	Long flame coal (−2 mm)	1573 K	180 min	Na_2CO_3: 17.1wt%	72.05%	77.27%
			1523 K	180 min	K_2CO_3: 22.01wt%	70.77%	92.39%
Huang *et al.* [108]	Red mud	Coal (−3 mm)	1423 K	180 min	Na_2CO_3: 3wt%, CaF_2: 3wt%	89.57%	91.15%
Chun *et al.* [109]	Red mud (−0.5 mm, 80wt%)	Bituminous coal (−1 mm)	1423 K	80 min	Na_2SO_4: 9wt%, CaO: 9.46wt%	90.28%	92.14%
Pan *et al.* [111]	Nickel slag (−75 μm, 88.16wt%)	Soft coal	1473 K	20 min	Coal: 5wt%, slag basicity: 0.15	75.26%	42.17%
Ma and Han [112]	Nickel slag (−2 mm)	Coal (−2 mm)	1573 K	60 min	Coal blending ratio: 4, CaO: 20wt%	89.84%	92.15%
Li *et al.* [30]	Oolitic iron ore (−2 mm)	Coal (−2 mm)	1473 K	60 min	Coal: 30wt%	92.53%	90.78%
Sun *et al.* [22]	Oolitic iron ore (−2 mm)	Coal (−2 mm)	1523 K	50 min	C/O mole ratio: 2.0, CaO: 10wt%	89.63%	96.21%
Ma *et al.* [57]	Oolitic iron ore (−74 μm)	Anthracite	1323 K	45 min	Anthracite: 24wt%	N. A	90.70%

6.1. Iron recovery by coal-based reduction

Copper slag is a waste with a high TFe grade, and iron can be effectively recovered through coal-based reduction. Li *et al.* [29] mixed copper slag and coke and then ground it to a fineness of −74 μm, accounting for 90wt%. CaO was used to promote the reduction of fayalite and hortonolite to enhance the recovery of TFe. Under ideal conditions, a nearly monophase metallic iron powder was obtained with TFe grade of 96.21% and TFe recovery of 91.82%. In other studies, the same processes, namely, coal-based reduction and magnetic separation process, were applied to recover iron from copper slag, and similar process indexes were obtained [103–104]. Zhou *et al.* [105] attempted to use walnut shells as a green reductant to reduce iron minerals in copper slag. They first prepared biochar from walnut shells at 873 K. Through reduction and magnetic separation of copper slag, an iron concentrate with an iron grade of 73.20wt% and iron recovery of 95.56wt% was obtained. Zhou *et al.* [105] proved that walnut shells can be used to achieve clean iron extraction from copper slag.

Red mud is a toxic waste of the industrial process that produces alumina, and it is characterized by a high pH range and iron content [106–107]. Zinoveev *et al.* [84] promoted the growth of metallic iron particles through the addition of 17.1wt% Na_2CO_3 and 22.01wt% K_2CO_3. They observed that K_2CO_3 can be used to obtain better process indexes of coal-based reduction and magnetic separation. Similarly, by adding 3wt% Na_2CO_3 and 3wt% CaF_2 to the red mud, Huang *et al.* [108] obtained a metallic iron powder with a TFe grade

of 89.57wt% and a TFe recovery of 91.15wt%. Chun *et al.* [109] used Na_2SO_4 and CaO as additives to prepare metallic iron powder with a TFe grade of 90.28% and a TFe recovery of 92.14% from red mud, which can replace scrap as the burden material of electric arc furnace steelmaking. Agrawal *et al.* [110] conducted the reduction roasting of red mud with charcoal in microwave and muffle furnaces and observed that the microwave can significantly increase the reduction rate and decrease the reductant consumption.

To recover nickel and iron from a nickel laterite ore, Yuan *et al.* [17] proposed a deep reduction and magnetic separation process. They noticed that appropriately increasing temperature was beneficial to the reduction and growth of nickel–iron particles, but an extremely high temperature melted the gangue minerals, which was disadvantageous to magnetic separation. The addition of CaO can improve the reduction of fayalite and promote the growth of nickel–iron particles. Under the best conditions, nickel–iron concentrate with a nickel grade of 6.96%, nickel recovery of 94.06%, TFe grade of 34.74%, and TFe recovery of 80.44% was obtained. In addition, nickel slag is a resource with a high TFe grade. Pan *et al.* [111] performed selective reduction of nickel slag to recover nickel, copper, and iron and added CaO to promote grain growth. They realized the selective recovery of nickel, copper, and iron. The grades of nickel, copper, and iron in the concentrate were 3.25%, 1.20%, and 75.26%, respectively, and the recoveries were 82.20%, 80.00%, and 42.17%, respectively. However, the P and sulfur contents in the concentrate were relatively high, and further research was needed to remove them. By contrast, Ma and Han [112] obtained better process indexes for the coal-based reduction and magnetic separation of nickel slag. The iron grade and recovery of the concentrate were 89.84wt% and 92.15wt%, respectively, and the recoveries of nickel, cobalt, and copper were more than 85wt%.

Coal-based reduction and magnetic separation processes are also often employed to extract iron from oolitic hematite ores. For oolitic hematite with P content <0.8wt%, by adding dephosphorization additives, the low-P (P content ≤0.05wt%) metallic iron powder that can be directly used for steelmaking can be obtained [22,30,57]. As for the oolitic hematite with P content >0.8wt%, by controlling the migration of P, the high-P (P content ≥1.5wt%) metallic iron powder can be obtained. The high-P metallic iron powder can be processed by smelting dephosphorization technology to obtain qualified liquid steel and high-P steel slag that can be directly used as phosphate fertilizer or acid soil conditioner [23,113]. To explore and utilize the enormous resources of oolitic iron ore in China, Li *et al.* [30] developed a laboratory technology of deep reduction. After optimizing the conditions of deep reduction and magnetic separation, Li *et al.* [30] obtained near-mono-phase iron powder with TFe grade and recovery of 92.53% and 90.78%, respectively. Sun *et al.* [22] carried out a coal-based reduction on a high-P oolitic hematite ore. Under the action of CaO, after coal-based reduction, the reduction product with a metallization degree of 95.82wt% was acquired. In addition, a low-P iron concentrate with a TFe grade of 89.63% and recovery of 96.21% was obtained by magnetic separation. Ma *et al.* [57] explored the application of microwave in the coal-based reduction of oolitic hematite ore. They observed that using microwave can significantly lower the reduction temperature. When the sample with 24wt% anthracite was reduced at 1323 K for 45 min, the metallization degree can reach 88.91wt%. Through magnetic separation, the TFe recovery reached 90.70%.

Numerous experimental results show that the coal-based reduction and magnetic separation process to recover iron from refractory iron-bearing resources is an efficient method that can realize the utilization of these resources. The iron recovery by coal-based reduction and magnetic separation is in the laboratory stage yet, and further industrialization experiments are still needed. The evaluations from various perspectives such as economy and environmental protection are required.

6.2. RHF

The design of RHF is based on coal-based, fast direct-reduction technology [114–115]. RHF was originally designed and built by Canadian International Nickel Corporation in 1978 and was named INMETCO [98]. Fig. 8 describes the schematic of RHF. In the process of coal-based reduction, the materials (usually pellets composed of fine iron ore powder and fine non-coking coal powder) are fed into the furnace through a feeding machine, with a thickness of one to two layers [97,118]. Most of the heat in the furnace is mainly maintained by the burner, and the fuel is usually natural gas, oil, etc. [118–119]. While the pellets rotate one circle in the furnace, the iron oxides are reduced by the coal and its gasification product CO [120]. The product is unloaded through the unloading screw. Currently, after years of development, RHF has been extensively applied in iron oxide reduction and attempted to be utilized in coal-based reduction [97].

Metallurgical plants will produce a considerable amount of dust and metallurgical waste during the production process, and these by-products usually contain large amounts of valuable metals, such as iron, chromium, and zinc [121]. Thus far, numerous companies have successfully used RHF coal-based reduction to efficiently recover these metals from by-products, such as Ma Steel, Sha Steel, and Lai Steel in China, Korea Zinc Co., Ltd. in Korea, and Nippon Steel and Kobe Steel in Japan [97–98]. In the practical production process, the metallization degree can usually be over 80wt%. Kawatra and co-authors [8,122] explored the conditions affecting the coal-based reduction of iron ore-coal pellets, including reduction time, reduction temperature, and so on. They conducted the coal-based reduction of iron ores by RHF to produce iron nuggets that can be easily ground to recover metallic iron by magnetic separation, achieving a TFe recovery of more than 80% [8]. The coal used in RHF may contain a large amount of volatiles, of which the main reducing substances are CO, H_2, and CH_4 [123]. Sohn and Fruehan [123] verified that the volatiles were beneficial to the re-

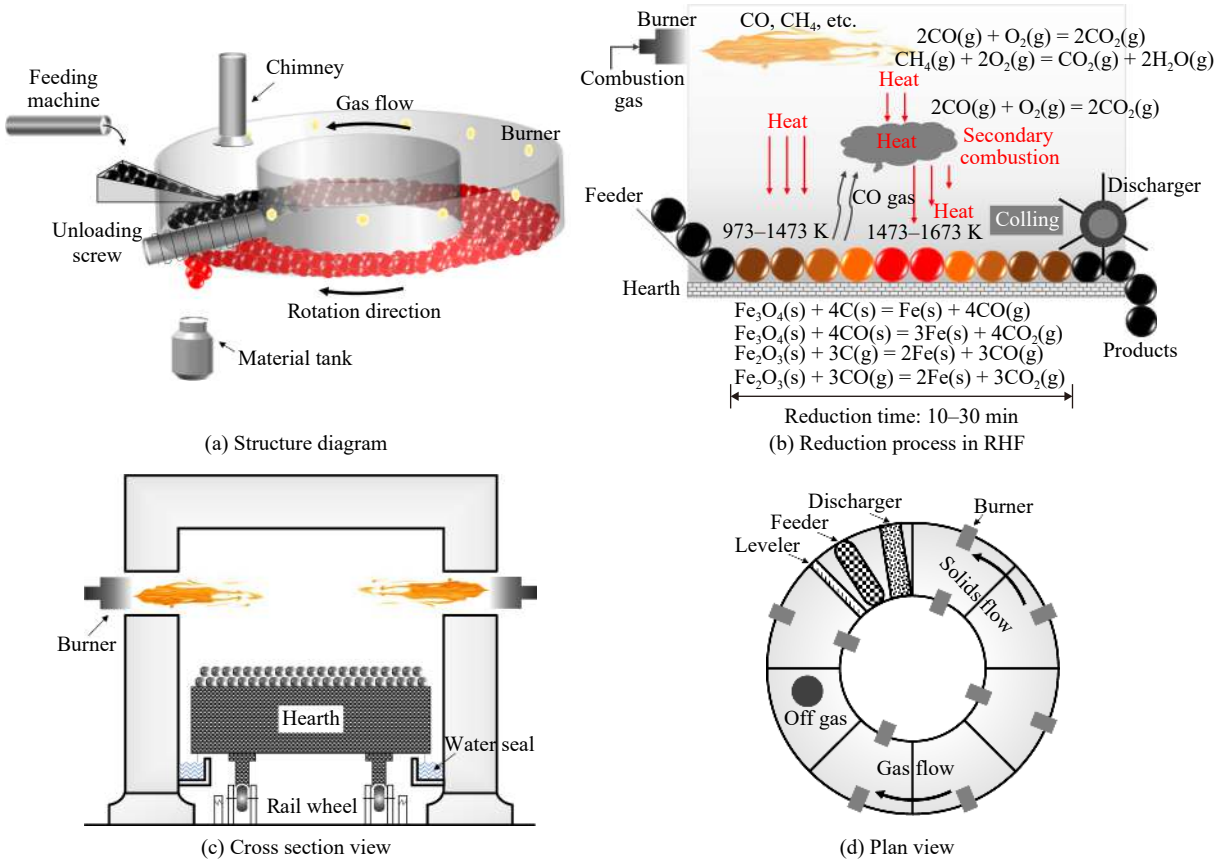

Fig. 8. Schematic of RHF [98,116–117].

duction of iron oxides, especially iron oxides on the top layer in RHF. They focused on the reduction kinetics of H_2. The reduction rate was initially controlled by nucleation and growth. The newly formed iron nucleus can catalyze the reduction. A mixture mechanism of chemical kinetics and pore diffusion controlled the reduction rate. Kumar *et al.* [116] carried out a thermodynamics analysis to estimate the CO_2 emissions from the coal-based reduction of iron ore in RHF. They analyzed the effects of different conditions on CO_2 emissions and established thermodynamics models, which helped to optimize the reduction process. Landfahrer *et al.* [124] developed a numerically efficient model using the computational fluid dynamics (CFD) method to optimize the combustion process in RHF. The measurement results showed a good agreement with the model predictions, which implied that this model can be feasibly applied to optimize the structure of RHF.

6.3. RK

RK is a common equipment for recovering iron from refractory iron ore by pyrometallurgy. Fig. 9 shows the schematic of RK, which can be divided into three parts in the axial direction. The raw materials are first preheated after entering the RK, and the temperature is generally below 600 K. During preheating, the adsorbed and crystal waters in raw materials are removed. In the reduction zone, the raw materials are gradually heated to the reaction temperature. Most iron oxides are reduced to metallic iron by coal and CO. Then, in the last zone, the metallic iron particles gradually aggregate together and expand into iron particles with a particle size suitable for magnetic separation. In addition, gangue minerals, ash, and additives form the slags.

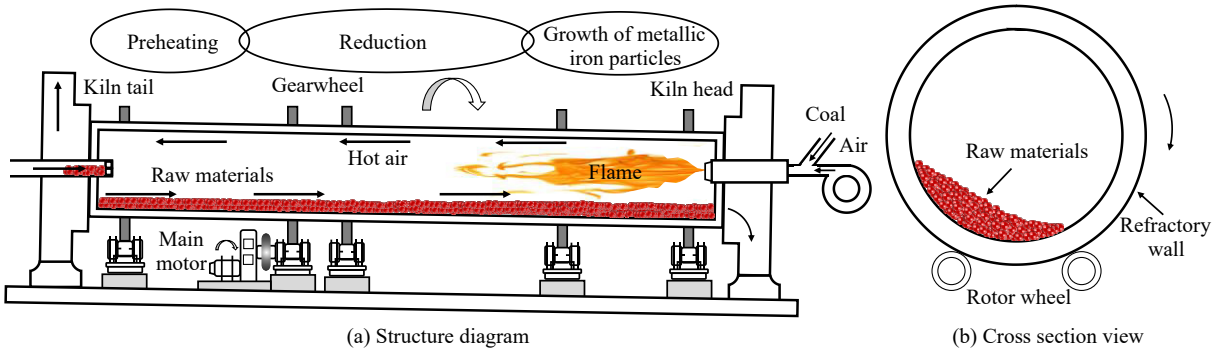

Fig. 9. Schematic of RK [100–102].

Zhong *et al.* [100] conducted a pilot scale coal-based reduction of low-TFe-grade iron ore. They considered that Fe_2O_3 was initially heated in the preheating zone of the RK, and most of it was reduced to Fe_3O_4 and FeO. Then, most Fe_3O_4 and FeO were reduced to Fe in the reduction zone. The research of Liang *et al.* [101] verified this reduction process. Finally, metallic iron particles gradually aggregated and grew. After grinding the metalized pellet to 90wt% with a size less than 0.045 mm, they efficiently recovered the iron powder through the magnetic separation with a TFe recovery of 85.61% and TFe grade of 92.04%. Using CFD, Liu *et al.* [125] established a three-dimensional steady-state mathematical model to analyze the reduction process in RK, thereby improving the product quality and productivity. The results showed that iron oxides were gradually reduced from Fe_2O_3 to Fe, and the reduction from FeO to Fe was the limiting step in the reduction of iron oxides because the reduction from FeO to Fe requires a higher reduction potential.

6.4. Critical development prospects

Notably, coal-based reduction and magnetic separation hewed out a new way for the efficient development and utilization of abundant refractory iron-bearing resources, which provided high-quality steelmaking raw materials. This process revitalized numerous iron resources and alleviated the supply pressure of iron ore. However, coal, as a typical fossil fuel, will yield greenhouse and pollution gases (carbon dioxide, sulfur dioxide, nitrogen oxides, etc.) in iron oxide reduction [126–128]. Furthermore, coal-based reduction must be carried out at a high temperature for a long time, and the maintenance of high temperature requires massive energy, which commonly comes from fossil fuels. Approximately 1.5–2.0 tons of CO_2 are emitted for every ton of metallic iron powder produced [129–131]. Overall, coal-based reduction is currently a technology with high CO_2 emissions, energy consumption, and high pollution, which is not conducive to the green and sustainable development of human society. Under the limits of the carbon neutrality target in the Paris Agreement and the CO_2 emissions restrictions of the world's major economies [126,132–133], the green and low-carbon development of coal-based reduction should be further explored.

Under the background that green and low-carbon development has become the consensus of most countries around the world, technological innovation aiming at reducing carbon dioxide emissions has become a new trend of green development in the steel industry [134–136]. Currently, substituting hydrogen for carbon-containing reductant is the main starting point for greening the steel industry [135,137–138]. The reduction of iron oxides by hydrogen emits water with zero CO_2 emissions. Compared with those for coal-based reduction, the kinetic conditions for hydrogen-based reduction were evidently improved owing to the increased mass transfer rate [139–141]. Therefore, for new participants in this field, replacing coal with H_2 is a bright prospect. At present, hydrogen-based reduction still has great limitations. Given the cost of hydrogen production, transportation and storage are relatively high, and the process of producing green hydrogen that leads to zero negative impact on the environment is at a low development level [135,142–143]. However, with the development of hydrogen production, storage, transportation technology, and the maturity of the green hydrogen production process (Fig. 10), hydrogen will be used on a large scale in human society, and hydrogen-based reduction will be extremely competitive.

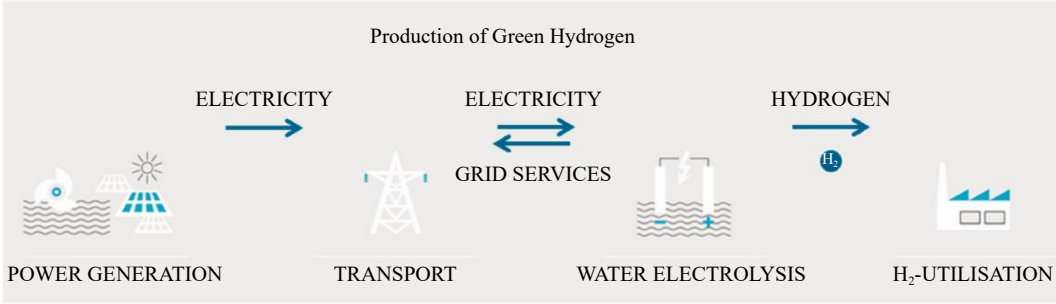

Fig. 10. Production of green hydrogen process relying on renewable energy to generate electricity to electrolyze water [144]. Reprinted from *J. Clean. Prod.*, 329, R.R. Wang, Y.Q. Zhao, A. Babich, D. Senk, and X.Y. Fan, Hydrogen direct reduction (H-DR) in steel industry—An overview of challenges and opportunities, art. No. 129797, Copyright 2021, with permission from Elsevier.

7. Conclusions and prospects

Through coal-based reduction and magnetic separation, iron can be recovered from refractory iron-bearing resources, which can alleviate the current consumption of high-grade iron ore resources. In this paper, coal-based reduction is reviewed from different perspectives, and the prospect of its development is critically discussed.

Hematite is gradually reduced to metallic iron in the rote of $Fe_2O_3 \rightarrow Fe_3O_4 \rightarrow FeO \rightarrow Fe$. In the reduction process, CO, the Boudouard reaction product of coal, dominates iron oxide reduction. The kinetic mechanisms of various reduction stages are different. In the initial reduction stage, the reduction is mainly controlled by the gas diffusion of CO and random nucleation mechanism, iron minerals are rapidly reduced, and the metallization degree increases rapidly. At this stage, the particle size of metallic iron particles is very small. Meanwhile, in the middle and last stages, the reduction is controlled by a mixture of multiple kinetic mechanisms, and the metallization degree does not increase. The metallic iron

particles gradually gather and grow into larger ones. In addition, temperature is the decisive factor for the growth of metallic iron particles.

Additives are usually used to improve coal-based reduction. They can react with gangue minerals and their intermediate products with wüstite, promote the Boudouard reaction of carbon, and improve the contact conditions between the sample and coal, promoting the reduction of iron oxides and increasing the process indexes. The micro-melting phase formed by the reaction between additives and gangue minerals can promote the diffusion and growth of metallic iron particles and significantly enhance the particle size. In addition, additives can be used for dephosphorization with three main mechanisms. Additives can inhibit the promoting effect of gangue minerals on the reduction of phosphorus minerals, destroy the ore structure and promote the separation of iron and phosphorus, or react with P-containing minerals to form water-soluble substances for dephosphorization by magnetic separation.

Iron can be feasibly recovered from refractory iron-bearing resources, such as copper slag, red mud, nickel slag, and oolitic hematite, by coal-based reduction and magnetic separation process. Iron concentrates with TFe grade and recovery of more than 80wt% can usually be obtained. In terms of the industrial application, the coal-based reduction industrial equipment can be developed based on existing pyrometallurgical equipment and the characteristics of RHF and RK with development potential be briefly introduced.

However, coal-based reduction, which consumes massive coal and energy, will cause numerous CO_2 emissions, which is not conducive to the realization of the low-carbon emission target of human society. In view of clean energy reduction is an emerging technology, using hydrogen or biomass to replace coal to reduce refractory iron-bearing resources is the future development direction, and it is expected to realize the low-carbon and green iron recovery from refractory iron-bearing resources.

Acknowledgements

This work was financially supported by the National Natural Science Foundation of China (No. 52022019), the National Key R&D Program of China (No. 2021YFC2901000), and the Fok Ying Tung Education Foundation (No. 161045).

Conflict of Interest

The authors declare no potential conflict of interest.

References

[1] J.X. Wu, J. Yang, L.W. Ma, Z. Li, and X.S. Shen, A system analysis of the development strategy of iron ore in China, *Resour. Policy*, 48(2016), p. 32.

[2] Q. Zhang, Y.S. Sun, Y.X. Han, Y.J. Li, and P. Gao, Effect of thermal oxidation pretreatment on the magnetization roasting and separation of refractory iron ore, *Miner. Process. Extr. Metall. Rev.*, 43(2022), No. 2, p. 182.

[3] X.L. Zhang, X.T. Gu, Y.X. Han, N. Parra-Álvarez, V. Claremboux, and S. K. Kawatra, Flotation of iron ores: A review, *Miner. Process. Extr. Metall. Rev.*, 42(2021), No. 3, p. 184.

[4] B. Anameric and S.K. Kawatra, Properties and features of direct reduced iron, *Miner. Process. Extr. Metall. Rev.*, 28(2007), No. 1, p. 59.

[5] D. Fernández-González, Í. Ruiz-Bustinza, J. Mochón, C. González-Gasca, and L. Verdeja, Iron ore sintering: Raw materials and granulation, *Miner. Process. Extr. Metall. Rev.*, 38(2017), No. 1, p. 36.

[6] X.L. Zhang, Y.X. Han, Y.S. Sun, Y. Lv, Y.J. Li and Z.D. Tang, An novel method for iron recovery from iron ore tailings with pre-concentration followed by magnetization roasting and magnetic separation, *Miner. Process. Extr. Metall. Rev.*, 41(2020), No. 2, p. 117.

[7] S.K. Roy, D. Nayak, and S.S. Rath, A review on the enrichment of iron values of low-grade Iron ore resources using reduction roasting-magnetic separation, *Powder Technol.*, 367(2020), p. 796.

[8] U. Srivastava and S.K. Kawatra, Strategies for processing low-grade iron ore minerals, *Miner. Process. Extr. Metall. Rev.*, 30(2009), No. 4, p. 361.

[9] Q. Zhang, Y.S. Sun, Y.X. Han, P. Gao, and Y.J. Li, Thermal decomposition kinetics of siderite ore during magnetization roasting, *Min. Metall. Explor.*, 38(2021), No. 3, p. 1497.

[10] R.A. Williams, Processing problematic ores, *Miner. Eng.*, 6(1993), No. 8-10, p. 809.

[11] X. Wang, B. Zhao, J. Liu, Y.M. Zhu, and Y.X. Han, Dithiouracil, a highly efficient depressant for the selective separation of molybdenite from chalcopyrite by flotation: Applications and mechanism, *Miner. Eng.*, 175(2022), art. No. 107287.

[12] S.K. Roy, D. Nayak, N. Dash, N. Dhawan, and S.S. Rath, Microwave-assisted reduction roasting–magnetic separation studies of two mineralogically different low-grade iron ores, *Int. J. Miner. Metall. Mater.*, 27(2020), No. 11, p. 1449.

[13] J.W. Yu, Y.X. Han, Y.J. Li, and P. Gao, Recent advances in magnetization roasting of refractory iron ores: A technological review in the past decade, *Miner. Process. Extr. Metall. Rev.*, 41(2020), No. 5, p. 349.

[14] K. Quast, A review on the characterisation and processing of oolitic iron ores, *Miner. Eng.*, 126(2018), p. 89.

[15] X.D. Xing, Y.L. Du, J.L. Zheng, Y.F. Chen, S. Ren, and J.T. Ju, Experimental study on strengthening carbothermic reduction of vanadium-titanium-magnetite by adding CaF_2, *Minerals*, 10(2020), No. 3, art. No. 219.

[16] P. Gao, G.F. Li, X.T. Gu, and Y.X. Han, Reduction kinetics and microscopic properties transformation of boron-bearing iron concentrate-carbon-mixed pellets, *Miner. Process. Extr. Metall. Rev.*, 41(2020), No. 3, p. 162.

[17] S. Yuan, W.T. Zhou, Y.J. Li, and Y.X. Han, Efficient enrichment of nickel and iron in laterite nickel ore by deep reduction and magnetic separation, *Trans. Nonferrous Met. Soc. China*, 30(2020), No. 3, p. 812.

[18] Y.J. Li, Y.X. Han, Y.M. Zhu, and J. Liu, Deep reduction tests of antelope iron ore in Linjiang area, *J. Northeast. Univ. Nat. Sci.*, 33(2012), No. 1, p. 137.

[19] Y.J. Li, Y.S. Sun, Y.X. Han and P. Gao, Coal-based reduction mechanism of low-grade laterite ore, *Trans. Nonferrous Met. Soc. China*, 23(2013), No. 11, p. 3428.

[20] Y.S. Sun, P. Gao, Y.X. Han, and D.Z. Ren, Reaction behavior of iron minerals and metallic iron particles growth in coal-based reduction of an oolitic iron ore, *Ind. Eng. Chem. Res.*, 52(2013), No. 6, p. 2323.

[21] Y.S. Sun, Y.X. Han, P. Gao, and G.F. Li, Investigation of kinetics of coal based reduction of oolitic iron ore, *Ironmaking*

Steelmaking, 41(2014), No. 10, p. 763.
[22] Y.S. Sun, Y.X. Han, P. Gao, Z.H. Wang, and D.Z. Ren, Recovery of iron from high phosphorus oolitic iron ore using coal-based reduction followed by magnetic separation, *Int. J. Miner. Metall. Mater.*, 20(2013), No. 5, p. 411.
[23] Y.S. Sun, Q. Zhang, Y.X. Han, P. Gao, and G.F. Li, Comprehensive utilization of iron and phosphorus from high-phosphorus refractory iron ore, *JOM*, 70(2018), No. 2, p. 144.
[24] W. Yu, T.C. Sun, Q. Cui, C.Y. Xu, and J. Kou, Effect of coal type on the reduction and magnetic separation of a high-phosphorus oolitic hematite ore, *ISIJ Int.*, 55(2015), No. 3, p. 536.
[25] Y.S. Sun, Y.X. Han, P. Gao, and Y.J. Li, Growth kinetics of metallic iron phase in coal-based reduction of oolitic iron ore, *ISIJ Int.*, 56(2016), No. 10, p. 1697.
[26] Y.S. Sun, Y.X. Han, P. Gao, and J.W. Yu, Size distribution behavior of metallic iron particles in coal-based reduction products of an oolitic iron ore, *Miner. Process. Extr. Metall. Rev.*, 36(2015), No. 4, p. 249.
[27] Y.S. Sun, Y.X. Han, Y.F. Li, and Y.J. Li, Formation and characterization of metallic iron grains in coal-based reduction of oolitic iron ore, *Int. J. Miner. Metall. Mater.*, 24(2017), No. 2, p. 123.
[28] Y.S. Sun, W.T. Zhou, Y.X. Han, and Y.J. Li, Effect of different additives on reaction characteristics of fluorapatite during coal-based reduction of iron ore, *Metals*, 9(2019), No. 9, art. No. 923.
[29] K.Q. Li, S. Ping, H.Y. Wang, and W. Ni, Recovery of iron from copper slag by deep reduction and magnetic beneficiation, *Int. J. Miner. Metall. Mater.*, 20(2013), No. 11, p. 1035.
[30] K.Q. Li, W. Ni, M. Zhu, M.J. Zheng, and Y. Li, Iron extraction from oolitic iron ore by a deep reduction process, *J. Iron Steel Res. Int.*, 18(2011), No. 8, p. 9.
[31] O.I. Nokhrina, I.D. Rozhihina, and I.E. Hodosov, The use of coal in a solid phase reduction of iron oxide, *IOP Conf. Ser.: Mater. Sci. Eng.*, 91(2015), art. No. 012045.
[32] Y. Haseli, Criteria for chemical equilibrium with application to methane steam reforming, *Int. J. Hydrogen Energy*, 44(2019), No. 12, p. 5766.
[33] D. Spreitzer and J. Schenk, Reduction of iron oxides with hydrogen—A review, *Steel Res. Int.*, 90(2019), No. 10, art. No. 1900108.
[34] N.S. Srinivasan, Reduction of iron oxides by carbon in a circulating fluidized bed reactor, *Powder Technol.*, 124(2002), No. 1-2, p. 28.
[35] A. Pineau, N. Kanari, and I. Gaballah, Kinetics of reduction of iron oxides by H_2: Part I: Low temperature reduction of hematite, *Thermochim. Acta*, 447(2006), No. 1, p. 89.
[36] W.K. Jozwiak, E. Kaczmarek, T.P. Maniecki, W. Ignaczak, and W. Maniukiewicz, Reduction behavior of iron oxides in hydrogen and carbon monoxide atmospheres, *Appl. Catal. A Gen.*, 326(2007), No. 1, p. 17.
[37] J.W. Chen, Y. Jiao, and X.D. Wang, Thermodynamic studies on gas-based reduction of vanadium titano-magnetite pellets, *Int. J. Miner. Metall. Mater.*, 26(2019), No. 7, p. 822.
[38] R. Béchara, H. Hamadeh, O. Mirgaux, and F. Patisson, Optimization of the iron ore direct reduction process through multiscale process modeling, *Materials* (*Basel*), 11(2018), No. 7, art. No. 1094.
[39] S. Mishra, Review on reduction kinetics of iron ore–coal composite pellet in alternative and sustainable ironmaking, *J. Sustain. Metall.*, 6(2020), No. 4, p. 541.
[40] S. Sun and W.K. Lu, A theoretical investigation of kinetics and mechanisms of iron ore reduction in an ore/coal composite, *ISIJ Int.*, 39(1999), No. 2, p. 123.
[41] Y.S. Sun, Y.X. Han, P. Gao, X.C. Wei, and G.F. Li, Thermogravimetric study of coal-based reduction of oolitic iron ore: Kinetics and mechanisms, *Int. J. Miner. Process.*, 143(2015), p. 87.
[42] H.M. Ahmed, N.N. Viswanathan, and B. Björkman, Isothermal reduction kinetics of self-reducing mixtures, *Ironmaking Steelmaking*, 44(2017), No. 1, p. 66.
[43] X.L. Yuan, F.M. Luo, S.F. Liu, M.Y. Zhang, and D.S. Zhou, Comparative study on the kinetics of the isothermal reduction of iron ore composite pellets using coke, charcoal, and biomass as reducing agents, *Metals*, 11(2021), No. 2, art. No. 340.
[44] A. Hammam, Y. Cao, A.H.A. El-Geassy, M.H. El-Sadek, Y. Li, H. Wei, M. Omran, and Y.W. Yu, Non-isothermal reduction kinetics of iron ore fines with carbon-bearing materials, *Metals*, 11(2021), No. 7, art. No. 1137.
[45] Y.S. Sun, Y.X. Han, X.C. Wei, and P. Gao, Non-isothermal reduction kinetics of oolitic iron ore in ore/coal mixture, *J. Therm. Anal. Calorim.*, 123(2016), No. 1, p. 703.
[46] R. Sah and S.K. Dutta, Kinetic studies of iron ore–coal composite pellet reduction by TG–DTA, *Trans. Indian Inst. Met.*, 64(2011), No. 6, p. 583.
[47] Z.C. Huang, K. Wu, B. Hu, H. Peng, and T. Jiang, Non-isothermal kinetics of reduction reaction of oxidized pellet under microwave irradiation, *J. Iron Steel Res. Int.*, 19(2012), No. 1, p. 1.
[48] M.C. Goswami, S. Prakash, and S.B. Sarkar, Kinetics of smelting reduction of fluxed composite iron ore pellets, *Steel Res.*, 70(1999), No. 2, p. 41.
[49] A.A. El-Geassy, M.H. Khedr, M.I. Nasr, and M.S. Aly, Behaviour of iron ore–fuel oil composite pellets in isothermal and non-isothermal reduction conditions, *Ironmaking Steelmaking*, 28(2001), No. 3, p. 237.
[50] A. Chatterjee, Role of particle size in mineral processing at Tata Steel, *Int. J. Miner. Process.*, 53(1998), No. 1-2, p. 1.
[51] T. Leißner, T. Mütze, K. Bachmann, S. Rode, J. Gutzmer, and U.A. Peuker, Evaluation of mineral processing by assessment of liberation and upgrading, *Miner. Eng.*, 53(2013), p. 171.
[52] H.Y. Tian, Z.Q. Guo, R.N. Zhan, J. Pan, D.Q. Zhu, C.C. Yang, L.T. Pan, and X.Z. Huang, Upgrade of nickel and iron from low-grade nickel laterite by improving direct reduction-magnetic separation process, *J. Iron Steel Res. Int.*, 29(2022), No. 8, p. 1164.
[53] P. Gao, Y.X. Han, Y.J. Li, and Y.S. Sun, Evaluation on deep reduction of iron ore based on digital image processing techniques, *J. Northeast. Univ. Nat. Sci.*, 33(2012), No. 1, p. 133.
[54] P. Gao, Y.S. Sun, D.Z. Ren, and Y.X. Han, Growth of metallic iron particles during coal-based reduction of a rare earths-bearing iron ore, *Min. Metall. Explor.*, 30(2013), No. 1, p. 74.
[55] J.W. Yu, Y.H. Qin, P. Gao, Y.S. Sun, and S.B. Ma, The growth characteristics and kinetics of metallic iron in coal-based reduction of Jinchuan ferronickel slag, *Minerals*, 11(2021), No. 8, art. No. 876.
[56] X.M. Li, Y. Li, X.Y. Zhang, Z.Y. Wen, and X.D. Xing, Growth characteristics of metallic iron particles in the direct reduction of nickel slag, *Metall. Mater. Trans. B*, 51(2020), No. 3, p. 925.
[57] Z.H. Ma, J.Z. Zhang, W. Li, and J. Chen, Study on deep reduction of oolitic hematite assisted with microwave radiation, *Adv. Mater. Res.*, 941-944(2014), p. 2574.
[58] H.Y. Zhao, Y.L. Chen, and X.Q. Duan, Study on the factors affecting the deep reduction of coal gangue containing high contents of iron and sulfur, *Fuel*, 288(2021), art. No. 119571.
[59] P. Gao, W.T. Zhou, Y.X. Han, Y.J. Li, and C.W. Zhang, Influence mechanisms of additives on coal-based reduction of complex refractory iron ore, *Miner. Process. Extr. Metall. Rev.*, 43(2022), No. 1, p. 1.
[60] C. Kamijo, M. Hoshi, T. Kawaguchi, H. Yamaoka, and Y.S. Kamei, Production of direct reduced iron by a sheet material inserting metallization method, *ISIJ Int.*, 41(2001), No. Suppl,

p. S13.
[61] S. Priyadarshi, S. Mishra, B. Kumar, and G.G. Roy, Effect of different forms of carbon on the reduction behaviour of iron ore-carbonaceous material composite pellets in multi-layer bed rotary hearth furnace (RHF), *Can. Metall. Q.*, 60(2021), No. 4, p. 281.
[62] Y.X. Han, Y.S. Sun, P. Gao, Y.J. Li, and Y.F. Mu, Particle size distribution of metallic iron during coal-based reduction of an oolitic iron ore, *Min. Metall. Explor.*, 31(2014), No. 3, p. 169.
[63] Y.S. Sun, Y.X. Han, P. Gao, and Y.F. Mu, Particle size measurement of metallic iron in reduced materials based on optical image analysis, *Chem. Eng. Technol.*, 37(2014), No. 12, p. 2030.
[64] X. Zhang, G.H. Li, M.J. Rao, H.P. Mi, B.J. Liang, J.X. You, Z.W. Peng, and T. Jiang, Growth of metallic iron particles during reductive roasting of boron-bearing magnetite concentrate, *J. Cent. South Univ.*, 27(2020), No. 5, p. 1484.
[65] H.F. Yang, L.L. Jing, and C.G. Dang, Iron recovery from copper-slag with lignite-based direct reduction followed by magnetic separation, *Chin. J. Nonferrous Met.*, 21(2011), No. 5, p. 1165.
[66] Y.Q. Zhao, T.C. Sun, and Z. Wang, Extraction of iron from refractory titanomagnetite by reduction roasting and magnetic separation, *ISIJ Int.*, 61(2021), No. 1, p. 93.
[67] L. Zhang, H.H. Chen, R.D. Deng, W.R. Zuo, B. Guo, and J.G. Ku, Growth behavior of iron grains during deep reduction of copper slag, *Powder Technol.*, 367(2020), p. 157.
[68] Y.X. Han, C.W. Zhang, Y.S. Sun, and P. Gao, Mechanism analysis on deep reduction of complex refractory iron ore promoted by Na_2CO_3, *J. Northeast. Univ. Nat. Sci.*, 33(2012), No. 11, p. 1633.
[69] H. Long, Q. Meng, T. Chun, P. Wang, and J. Li, Preparation of metallic iron powder from copper slag by carbothermic reduction and magnetic separation, *Can. Metall. Q.*, 55(2016), No. 3, p. 338.
[70] D.C. Fan, W. Ni, J.Y. Wang, and K. Wang, Effects of CaO and Na_2CO_3 on the reduction of high silicon iron ores, *J. Wuhan Univ. Technol. Mater Sci Ed*, 32(2017), No. 3, p. 508.
[71] T. Jiang, S.F. Guan, Y. Xia, S.W. Yu, X.X. Xue, R.G. Bai, D.H. Chen, and F.Z. Chang, Research on the coal-based direct reduction of vanadium titanomagenetite, *Adv. Mater. Res.*, 753-755(2013), p. 16.
[72] Y.S. Sun, Y.F. Li, Y.X. Han, and Y.J. Li, Migration behaviors and kinetics of phosphorus during coal-based reduction of high-phosphorus oolitic iron ore, *Int. J. Miner. Metall. Mater.*, 26(2019), No. 8, p. 938.
[73] Y.Y. Zhang, Q.G. Xue, G. Wang, and J.S. Wang, Gasification and migration of phosphorus from high-phosphorus iron ore during carbothermal reduction, *ISIJ Int.*, 58(2018), No. 12, p. 2219.
[74] S.C. Wu, Z.Y. Li, T.C. Sun, J. Kou, and X.H. Li, Effect of additives on iron recovery and dephosphorization by reduction roasting–magnetic separation of refractory high-phosphorus iron ore, *Int. J. Miner. Metall. Mater.*, 28(2021), No. 12, p. 1908.
[75] H.F. Yang, L.L. Jing, and B.G. Zhang, Recovery of iron from vanadium tailings with coal-based direct reduction followed by magnetic separation, *J. Hazard. Mater.*, 185(2011), No. 2-3, p. 1405.
[76] S.J. Bai, S.M. Wen, D.W. Liu, W.B. Zhang, and Q.B. Cao, Beneficiation of high phosphorus limonite ore by sodium-carbonate-added carbothermic reduction, *ISIJ Int.*, 52(2012), No. 10, p. 1757.
[77] W. Yu, T.C. Sun, J. Kou, Y.X. Wei, C.Y. Xu, and Z.Z. Liu, The function of $Ca(OH)_2$ and Na_2CO_3 as additive on the reduction of high-phosphorus oolitic hematite-coal mixed pellets, *ISIJ Int.*, 53(2013), No. 3, p. 427.
[78] D.Q. Zhu, T.J. Chun, J. Pan, L.M. Lu, and Z. He, Upgrading and dephosphorization of Western Australian iron ore using reduction roasting by adding sodium carbonate, *Int. J. Miner. Metall. Mater.*, 20(2013), No. 6, p. 505.
[79] A. Basumallick, Influence of CaO and Na_2CO_3 as additive on the reduction of hematite–lignite mixed pellets, *ISIJ Int.*, 35(1995), No. 9, p. 1050.
[80] S.J. Bai, C. Lv, S.M. Wen, D.W. Liu, W.B. Zhang, and Q.B. Cao, Effects of sodium carbonate on the carbothermic reduction of siderite ore with high phosphorus content, *Min. Metall. Explor.*, 30(2013), No. 2, p. 100.
[81] Z. Zulhan and W. Shalat, Evolution of ferronickel particles during the reduction of low-grade saprolitic laterite nickel ore by coal in the temperature range of 900–1250°C with the addition of $CaO–CaF_2–H_3BO_3$, *Int. J. Miner. Metall. Mater.*, 28(2021), No. 4, p. 612.
[82] W. Ding, J.H. Xiao, Y. Peng, S.Y. Shen, and T. Chen, Iron extraction from red mud using roasting with sodium salt, *Miner. Process. Extr. Metall. Rev.*, 42(2021), No. 3, p. 153.
[83] G.H. Li, S.H. Zhang, M.J. Rao, Y.B. Zhang, and T. Jiang, Effects of sodium salts on reduction roasting and Fe–P separation of high-phosphorus oolitic hematite ore, *Int. J. Miner. Process.*, 124(2013), p. 26.
[84] D. Zinoveev, P. Grudinsky, A. Zakunov, A. Semenov, M. Panova, D. Valeev, A. Kondratiev, V. Dyubanov, and A. Petelin, Influence of Na_2CO_3 and K_2CO_3 addition on iron grain growth during carbothermic reduction of red mud, *Metals*, 9(2019), No. 12, art. No. 1313.
[85] P.I. Grudinskii, V.G. Dyubanov, D.V. Zinoveev, and M.V. Zheleznyi, Solid-phase reduction and iron grain growth in red mud in the presence of alkali metal salts, *Russ. Metall. Met.*, 2018(2018), No. 11, p. 1020.
[86] Y.Q. Zhao, T.C. Sun, H.Y. Zhao, X.H. Li, and X.P. Wang, Effects of $CaCO_3$ as additive on coal-based reduction of high-phosphorus oolitic hematite ore, *ISIJ Int.*, 58(2018), No. 10, p. 1768.
[87] S.I. Rudyuk, É.I. Fel'dman, E.I. Chernov, and V.F. Korobeinik, Effect of sulfur and phosphorus on the properties of steel 18B, *Met. Sci. Heat Treat.*, 16(1974), No. 12, p. 1056.
[88] V. Shankar, T.P.S. Gill, S.L. Mannan, and S. Sundaresan, Solidification cracking in austenitic stainless steel welds, *Sādhanā*, 28(2003), No. 3-4, p. 359.
[89] M.S. Najjar and D.Y. Jung, High temperature desulfurization of synthesis gas with iron compounds, *Fuel Process. Technol.*, 44(1995), No. 1-3, p. 173.
[90] J.P. Jin, W.T. Zhou, Y.S. Sun, Y.X. Han, and Y.J. Li, Reaction characteristics and existing form of phosphorus during coal-based reduction of oolitic iron ore, *Minerals*, 11(2021), No. 3, art. No. 247.
[91] S.C. Wu, Z.Y. Li, T.C. Sun, J. Kou, and C.Y. Xu, The mechanism of $CaCO_3$ in the gas-based direct reduction of a high-phosphorus oolitic iron ore, *Physicochem. Probl. Miner. Process.*, 57(2021), No. 4, p. 117.
[92] S.J. Bai, S.M. Wen, D.W. Liu, W.B. Zhang, and Y.J. Xian, Catalyzing carbothermic reduction of siderite ore with high content of phosphorus by adding sodium carbonate, *ISIJ Int.*, 51(2011), No. 10, p. 1601.
[93] Y.L. Li, T.C. Sun, C.Y. Xu, and Z.H. Liu, New dephosphorizing agent for phosphorus removal from high-phosphorus oolitic hematite ore in direct reduction roasting, *J. Cent. South Univ. Sci. Technol.*, 43(2012), No. 3, p. 827.
[94] C.Y. Xu, T.C. Sun, J. Kou, Y.L Li, X.L Mo, and L.G Tang, Mechanism of phosphorus removal in beneficiation of high phosphorous oolitic hematite by direct reduction roasting with dephosphorization agent, *Trans. Nonferrous Met. Soc. China*, 22(2012), No. 11, p. 2806.

[95] Y. Xu, T.C. Sun, Z.G. Liu, and C.Y. Xu, Phosphorus occurrence state and phosphorus removal research of a high phosphorous oolitic hematite by direct reduction roasting method, *J. Northeast. Univ. Nat. Sci.*, 34(2013), No. 11, p. 1651.

[96] D.W. Yang, T.C. Sun, H.F. Yang, C.Y. Xu, C.Y. Qi, and Z.X. Li, Dephosphorization mechanism in a roasting process for direct reduction of high-phosphorus oolitic hematite in west Hubei Province, China, *J. Univ. Sci. Technol. Beijing*, 32(2010), No. 8, p. 968.

[97] H. Ishikawa, J. Kopfle, J. McClelland, and J. Ripke, Rotary hearth furnace technologies for iron ore and recycling applications, *Arch. Metall. Mater.*, 53(2008), No. 2, p. 541.

[98] Y.Y. Zhang, Y.H. Qi, Z.S. Zou, and Y.G. Li, Development prospect of rotary hearth furnace process in China, *Adv. Mater. Res.*, 746(2013), p. 533.

[99] J. Zhang, H.M. Zhou, Y.H. Qi, and D.L. Yan, *A Kind of Iron-making Method of Carbon-thermal Pre-reduction, Gas-based Deep Reduction and Synchronous Cooling*, Chinese Patent, Appl. 202010246783.7, 2020.

[100] R.H. Zhong, L.Y. Yi, Z.C. Huang, W. Cai, and X. Jiang, Highly efficient beneficiation of low-grade iron ore via ore–coal composite-fed rotary kiln reduction: Pilot-scale study, *JOM*, 72(2020), No. 4, p. 1680.

[101] Z.K. Liang, L.Y. Yi, Z.C. Huang, B. Lu, X. Jiang, W. Cai, B.Z. Tian, and Y.Y. Jin, Insight of iron ore-coal composite reduction in a pilot scale rotary kiln: A post-mortem study, *Powder Technol.*, 356(2019), p. 691.

[102] H. Tsuji, Behavior of reduction and growth of metal in smelting of saprolite Ni-ore in a rotary kiln for production of ferronickel alloy, *ISIJ Int.*, 52(2012), No. 6, p. 1000.

[103] H.Y. Wang, K.Q. Li, W. Ni, X.Y. Huang, and Y. Jia, Experimental research of deep reduction and magnetic separation process of a high-iron copper slag, *Met. Mine*, 41(2012), No. 11, p. 141.

[104] S. Wang, W. Ni, C.L. Wang, D.Z. Li, and H.Y. Wang, Study of deep reduction process for iron recovery from copper slag tailings, *Met. Mine*, 43(2014), No. 3, p. 156.

[105] S.W. Zhou, Y.G. Wei, B. Li, and H. Wang, Cleaner recycling of iron from waste copper slag by using walnut shell char as green reductant, *J. Clean. Prod.*, 217(2019), p. 423.

[106] M. Archambo and S.K. Kawatra, Red mud: Fundamentals and new avenues for utilization, *Miner. Process. Extr. Metall. Rev.*, 42(2021), No. 7, p. 427.

[107] X. Liu, Y.X. Han, F.Y. He, P. Gao, and S. Yuan, Characteristic, hazard and iron recovery technology of red mud—A critical review, *J. Hazard. Mater.*, 420(2021), art. No. 126542.

[108] Z.C. Huang, L.B. Cai, Y.B. Zhang, Y.B. Yang, and T. Jiang, Reduction of iron oxides of red mud reinforced by Na_2CO_3 and CaF_2, *J. Cent. South Univ. Sci. Technol.*, 41(2010), No. 3, p. 838.

[109] T.J. Chun, D.Q. Zhu, J. Pan, and Z. He, Preparation of metallic iron powder from red mud by sodium salt roasting and magnetic separation, *Can. Metall. Q.*, 53(2014), No. 2, p. 183.

[110] S. Agrawal, V. Rayapudi, and N. Dhawan, Comparison of microwave and conventional carbothermal reduction of red mud for recovery of iron values, *Miner. Eng.*, 132(2019), p. 202.

[111] J. Pan, G.L. Zheng, D.Q. Zhu, and X.L. Zhou, Utilization of nickel slag using selective reduction followed by magnetic separation, *Trans. Nonferrous Met. Soc. China*, 23(2013), No. 11, p. 3421.

[112] S.B. Ma, and Y.X. Han, Study of extracting valuable metals from nickel smelting slag by a coal-based reduction method, *J. China Univ. Min. Technol.*, 43(2014), No. 2, p. 305.

[113] P. Gao, G.F. Li, Y.X. Han, and Y.S. Sun, Reaction behavior of phosphorus in coal-based reduction of an oolitic hematite ore and pre-dephosphorization of reduced iron, *Metals*, 6(2016), No. 4, art. No. 82.

[114] L. Li, Study on acid hydrolysis process of deep reduction slag of panzhihua V-timagnetite, *Inorg. Chem. Ind.*, 42(2010), No. 6, p. 52.

[115] Z.C. Cao, T.C. Sun, X. Xue, and Z.H. Liu, Iron recovery from discarded copper slag in a RHF direct reduction and subsequent grinding/magnetic separation process, *Minerals*, 6(2016), No. 4, art. No. 119.

[116] S. Liang, X.P. Liang, and Q. Tang, Treatment of secondary dust produced in rotary hearth furnace through alkali leaching and evaporation–crystallization processes, *Processes*, 8(2020), No. 4, art. No. 396.

[117] H. Tsutsumi, S. Yoshida, and M. Tetsumoto, Features of FASTMET process, *KOBELCO Technol. Rev.*, 2010, No. 29, p. 85.

[118] B. Kumar, S. Mishra, G.G. Roy, and P.K. Sen, Estimation of carbon dioxide emissions in rotary hearth furnace using a thermodynamic model, *Steel Res. Int.*, 88(2017), No. 5, art. No. 1600265.

[119] S.H. Zhang, G. Wang, H. Zhang, J.S. Wang, and Q.G. Xue, Effect of gangue composition on iron nugget production from iron ore–coal composite pellet, *J. Iron Steel Res. Int.*, 26(2019), No. 9, p. 917.

[120] T. Matsumura, Y. Takenaka, M. Shimizu, T. Negami, I. Kobayashi, and A. Uragami, The reduction and melting behavior of carbon composite iron ore pellet on high temperature, *Tetsu-to-Hagane*, 84(1998), No. 6, p. 405.

[121] B. Das, S. Prakash, P.S.R. Reddy, and V.N. Misra, An overview of utilization of slag and sludge from steel industries, *Resour. Conserv. Recycl.*, 50(2007), No. 1, p. 40.

[122] B. Anameric and S.K. Kawatra, Laboratory study related to the production and properties of pig iron nuggets, *Min. Metall. Explor.*, 23(2006), No. 1, p. 52.

[123] I. Sohn and R.J. Fruehan, The reduction of iron oxides by volatiles in a rotary hearth furnace process: Part I. The role and kinetics of volatile reduction, *Metall. Mater. Trans. B*, 36(2005), No. 5, p. 605.

[124] M. Landfahrer, C. Schluckner, R. Prieler, H. Gerhardter, T. Zmek, J. Klarner, and C. Hochenauer, Development and application of a numerically efficient model describing a rotary hearth furnace using CFD, *Energy*, 180(2019), p. 79.

[125] C.H. Liu, X.Y. Ding, H.G. Liu, X.L Yan, C. Dong, and J. Wang, Numerical analysis on characteristics of reduction process within a pre-reduction rotary kiln, *Metals*, 11(2021), No. 8, art. No. 1180.

[126] B.A. Gyamfi, F.F. Adedoyin, M.A. Bein, F.V. Bekun, and D.Q. Agozie, The anthropogenic consequences of energy consumption in E7 economies: Juxtaposing roles of renewable, coal, nuclear, oil and gas energy: Evidence from panel quantile method, *J. Clean. Prod.*, 295(2021), art. No. 126373.

[127] O. Kanat, Z. Yan, M.M. Asghar, Z. Ahmed, H. Mahmood, D. Kirikkaleli, and M. Murshed, Do natural gas, oil, and coal consumption ameliorate environmental quality? Empirical evidence from Russia, *Environ. Sci. Pollut. Res. Int.*, 29(2022), No. 3, p. 4540.

[128] D. Cholico-González, N.O. Lara, M.A.S. Miranda, R.M. Estrella, R.E. García, and C.A. León Patiño, Efficient metallization of magnetite concentrate by reduction with agave bagasse as a source of reducing agents, *Int. J. Miner. Metall. Mater.*, 28(2021), No. 4, p. 603.

[129] J.P. Birat, J.P. Vizioz, Y. de Lassat de Pressigny, M. Schneider, and M. Jeanneau, CO_2 emissions and the steel industry's available responses to the greenhouse effect, *Rev. Met. Paris*, 96(1999), No. 10, p. 1203.

[130] V.G. Lisienko, Y.N. Chesnokov, A.V. Lapteva, and V.Y. Noskov, Types of greenhouse gas emissions in the production of cast iron and steel, *IOP Conf. Ser.: Mater. Sci. Eng.*, 150(2016), art. No. 012023.

[131] Q.Q. Chen, Y. Gu, Z.Y. Tang, W. Wei, and Y.H. Sun, Assessment of low-carbon iron and steel production with CO_2 recycling and utilization technologies: A case study in China, *Appl. Energy*, 220(2018), p. 192.

[132] W.R. Zhang, Y.O. Zhou, Z. Gong, J.J Kang, C.H Zhao, Z.X Meng, J. Zhang, T. Zhang, and J.H Yuan, Quantifying stranded assets of the coal-fired power in China under the Paris Agreement target, *Clim. Policy*, 2021. DOI: 10.1080/14693062.2021.1953433

[133] Q.F. Guo, X. Xi, S.T. Yang, and M.F. Cai, Technology strategies to achieve carbon peak and carbon neutrality for China's metal mines, *Int. J. Miner. Metall. Mater.*, 29(2022), No. 4, p. 626.

[134] L. Ren, S. Zhou, T.D. Peng, and X.M. Ou, A review of CO_2 emissions reduction technologies and low-carbon development in the iron and steel industry focusing on China, *Renewable Sustainable Energy Rev.*, 143(2021), art. No. 110846.

[135] J. Tang, M.S. Chu, F. Li, C. Feng, Z.G. Liu, and Y.S. Zhou, Development and progress on hydrogen metallurgy, *Int. J. Miner. Metall. Mater.*, 27(2020), No. 6, p. 713.

[136] L.Y. Liu, H.G. Ji, X.F. Lü, T. Wang, S. Zhi, F. Pei, and D.L Quan, Mitigation of greenhouse gases released from mining activities: A review, *Int. J. Miner. Metall. Mater.*, 28(2021), No. 4, p. 513.

[137] K. Rechberger, A. Spanlang, A. Sasiain Conde, H. Wolfmeir, and C. Harris, Green hydrogen-based direct reduction for low-carbon steelmaking, *Steel Res. Int.*, 91(2020), No. 11, art. No. 2000110.

[138] Y.B. Chen, W.G. Liu, and H.B. Zuo, Phosphorus reduction behavior of high-phosphate iron ore during hydrogen-rich sintering, *Int. J. Miner. Metall. Mater.*, 29(2022), No. 10, p. 1862.

[139] A. Bhaskar, M. Assadi, and H.N. Somehsaraei, Decarbonization of the iron and steel industry with direct reduction of iron ore with green hydrogen, *Energies*, 13(2020), No. 3, art. No. 758.

[140] Z.Y. Chen, C. Zeilstra, J. van der Stel, J. Sietsma, and Y.X. Yang, Review and data evaluation for high-temperature reduction of iron oxide particles in suspension, *Ironmak. Steelmak.*, 47(2020), No. 7, p. 741.

[141] Z.Y. Chen, J. Dang, X.J. Hu, and H.Y. Yan, Reduction kinetics of hematite powder in hydrogen atmosphere at moderate temperatures, *Metals*, 8(2018), No. 10, art. No. 751.

[142] A.G. Olabi, A.S. bahri, A.A. Abdelghafar, A. Baroutaji, E.T. Sayed, A.H. Alami, H. Rezk, and M. A. Abdelkareem, Large-vscale hydrogen production and storage technologies: Current status and future directions, *Int. J. Hydrogen Energy*, 46(2021), No. 45, p. 23498.

[143] C. Tarhan and M.A. Çil, A study on hydrogen, the clean energy of the future: Hydrogen storage methods, *J. Energy Storage*, 40(2021), art. No. 102676.

[144] R.R. Wang, Y.Q. Zhao, A. Babich, D. Senk, and X.Y. Fan, Hydrogen direct reduction (H-DR) in steel industry—An overview of challenges and opportunities, *J. Clean. Prod.*, 329(2021), art. No. 129797.